Paleoceanography and Paleoclimatology

AGU ADVANCING EARTH AND SPACE SCIENCES

RESEARCH ARTICLE
10.1029/2022PA004571

Evaluating the Drivers of Quaternary Dust Fluxes to the Western North Pacific: East Asian Dustiness and Northern Hemisphere Gustiness

Jordan T. Abell[1,2,3], Gisela Winckler[1,2], Alex Pullen[4], Christopher W. Kinsley[5,6], Paul A. Kapp[3], Jennifer L. Middleton[1], Frank J. Pavia[7], David McGee[5], Heather L. Ford[8], and Maureen E. Raymo[1,2]

[1]Lamont-Doherty Earth Observatory, Columbia University, Palisades, NY, USA, [2]Department of Earth and Environmental Sciences, Columbia University, New York, NY, USA, [3]Department of Geosciences, University of Arizona, Tucson, AZ, USA, [4]Department of Environment Engineering and Earth Sciences, Clemson University, Clemson, SC, USA, [5]Department of Earth, Atmospheric and Planetary Sciences, Massachusetts Institute of Technology, Cambridge, MA, USA, [6]Berkeley Geochronology Center, Berkeley, CA, USA, [7]Division of Geological and Planetary Sciences, California Institute of Technology, Pasadena, CA, USA, [8]School of Geography, Queen Mary University of London, London, UK

Key Points:

- Constant flux proxy-derived glacial dust fluxes to the North Pacific decrease between the early and late Quaternary
- Reduced glacial dust fluxes may be a result of shifting dust production dynamics and/or atmospheric circulation
- Chinese Loess Plateau accumulation rates may need to be reevaluated when considered for paleoclimate reconstructions

Supporting Information:

Supporting Information may be found in the online version of this article.

Correspondence to:

J. T. Abell,
joa423@lehigh.edu

Citation:

Abell, J. T., Winckler, G., Pullen, A., Kinsley, C. W., Kapp, P. A., Middleton, J. L., et al. (2023). Evaluating the drivers of Quaternary dust fluxes to the western North Pacific: East Asian dustiness and Northern Hemisphere gustiness. *Paleoceanography and Paleoclimatology*, *38*, e2022PA004571. https://doi.org/10.1029/2022PA004571

Received 20 OCT 2022
Accepted 14 AUG 2023

Author Contributions:

Conceptualization: Jordan T. Abell, Gisela Winckler, Alex Pullen, Paul A. Kapp, Jennifer L. Middleton, Frank J. Pavia
Data curation: Jordan T. Abell, Christopher W. Kinsley, Heather L. Ford
Formal analysis: Jordan T. Abell, Christopher W. Kinsley, Jennifer L. Middleton, Heather L. Ford
Funding acquisition: Jordan T. Abell, Gisela Winckler, Heather L. Ford, Maureen E. Raymo
Investigation: Jordan T. Abell

Abstract Quantifying variability in, and identifying the mechanisms behind, East Asian dust production and transport across the last several million years is essential for constraining future dust emissions and deposition. Our current understanding of East Asian dust dynamics through the Quaternary is primarily limited to low-resolution records from the North Pacific Ocean, those from the Chinese Loess Plateau (CLP), and paleoenvironmental reconstructions from arid basins. All are susceptible to sediment winnowing and focusing as well as input of poorly constrained or unidentified non-dust detrital material. To avoid these limitations, we examine high-resolution, constant flux proxy-derived dust fluxes from the North Pacific and find evidence for higher glacial dust fluxes in the late Pliocene-early Pleistocene compared to the late Pleistocene-Holocene. Our results suggest decreasing dust transported to the mid-latitude North Pacific Ocean from eastern Asia across the Quaternary. This observation is ostensibly at odds with previous dust records from marine sediments and the CLP, and with the perception of higher East Asian dust production and transport during the late Pleistocene associated with the amplification of glaciations. We provide three possible scenarios to describe the ∼2,700-ky evolution of eastern Asia glacial dust dynamics, and discuss them in the context of sediment production, availability, and atmospheric circulation. Our data and proposed driving mechanisms not only raise questions about the framework typically used to interpret dust archives from East Asia and the North Pacific Ocean, but also provide a roadmap for hypothesis testing and future work necessary to produce better-constrained records of paleo-dust fluxes.

1. Introduction

East Asia is one of the three largest dust emitting regions on the planet today (Kok et al., 2021; Tanaka & Chiba, 2006), with lithogenic dust originating from multiple desert areas, such as the Taklamakan, Junggar, Gobi, Badain Jaran, Mu Us, Tengger, and Hexi Corridor (Figure 1) (Laurent et al., 2005; X.-Y. Zhang et al., 2003). Dust from these regions is primarily transported eastward to the Chinese Loess Plateau (CLP), the North Pacific Ocean, North America, Greenland, with a small portion even returning to East Asia (Uno et al., 2009). This wind-blown dust can impact the planet's radiative forcing (Miller et al., 2014) and ocean biogeochemistry (Tagliabue et al., 2017). The dynamics of East Asian dust production have been shown to vary on millennial timescales (Nagashima et al., 2011), orbital timescales (Serno et al., 2017), across the Plio-Pleistocene boundary (Abell et al., 2021; Y. Sun & An, 2005), and throughout the Cenozoic (Anderson et al., 2020; Janecek & Rea, 1983; Lee et al., 2022; Rea et al., 1998; W. Zhang et al., 2016) in response to changes in climate and tectonics. However, the evolution of dust through the Quaternary, a period encapsulating substantially different and alternating climate states, has yet to be fully explored for East Asia, particularly at high resolution and with consideration for the combined effects of both varying surficial geology and climate. Considering the regional and global importance of windblown dust from East Asia, and its identified variability through time, it is critical to address this knowledge gap.

Methodology: Jordan T. Abell, Gisela Winckler, Christopher W. Kinsley, Heather L. Ford
Visualization: Jordan T. Abell
Writing – original draft: Jordan T. Abell, Gisela Winckler, Alex Pullen, Paul A. Kapp
Writing – review & editing: Jordan T. Abell, Gisela Winckler, Alex Pullen, Christopher W. Kinsley, Paul A. Kapp, Jennifer L. Middleton, Frank J. Pavia, David McGee, Heather L. Ford, Maureen E. Raymo

Many available data sets guiding our understanding of Quaternary East Asian dust production consist of grain-size measurements and sediment mass accumulation rates (MARs) on the CLP (e.g., Y. Sun & An, 2005; D. Sun et al., 2008; Y. Sun et al., 2010; J. Zhang et al., 2022) as well as dust flux records from the Sea of Japan and North Pacific Ocean (e.g., Anderson et al., 2020; Haug et al., 1995; Lee et al., 2022; Rea et al., 1998; Q. Zhang et al., 2020a). Like the data sets presented here, each of these has its own limitations. For example, spatial heterogeneity, wind erosion, changes in surface roughness and vegetation (i.e., the capacity to capture and emit dust), and internal recycling of sediments in the CLP complicates the usefulness of grain-size and MAR reconstructions to address synoptic dust dynamics, and challenges assumptions that the CLP provides a purely depositional archive (Ding et al., 2005; Kapp et al., 2015; Licht et al., 2016; Lu et al., 2019a; Stevens et al., 2018; H. Zhang et al., 2021). The uncertainty pertaining to Pleistocene dust production is exacerbated when low dust-emitting regions today are considered as major dust sources in the past. These include, but are not necessarily limited to, the Qaidam Basin (Kapp et al., 2011; Pullen et al., 2011), Yellow River floodplain (Nie et al., 2015), Hami Basin (Abell et al., 2020b; D. Zhang et al., 2020, 2022), and CLP (Kapp et al., 2015; Licht et al., 2016; Stevens et al., 2018). Similarly, for marine sediment cores, the incorporation of sediment redistributed by bottom currents into age model-derived sediment accumulation rates complicates records of dust that have been previously used to explain East Asian dust dynamics across the Pleistocene (Abell et al., 2021; Anderson et al., 2020; Lee et al., 2022; Rea et al., 1998; Q. Zhang et al., 2020a).

With these ambiguities in mind, high-resolution reconstructions of dust deposition during both the early and late Pleistocene from areas where reliable age models are available, continuous accumulation occurs, and methods correcting for sediment redistribution can be applied, are essential for answering questions regarding long-term changes to the mechanisms which underlie East Asian dust production, transport, and accumulation. To investigate the evolution of the dust systematics of East Asia from the late Pliocene-early Pleistocene to today, we compare two high-resolution dust proxy data sets that span the late Pleistocene–Holocene (~0–330 ka; Kinsley, 2019; Kinsley et al., 2022) and the late Pliocene = early Pleistocene (~2,500–2,730 ka; Abell et al., 2021) from the same, relatively well-dated North Pacific sediment core (Ocean Drilling Program (ODP) 1208; Figure 1). Unique to these data sets is the application of constant flux proxies (CFPs; specifically ^{230}Th and ^{3}He) to both time intervals, which permits determination of the vertical MARs of dust to the seafloor while accounting for syn-depositional sediment redistribution (Costa et al., 2020; McGee & Mukhopadhyay, 2013). Additionally, while these isotopes of Th and He can be used to reconstruct sediment fluxes, additional isotopes of each element (^{232}Th and ^{4}He) have also been shown to predominantly reflect detrital material in marine sediments, and as such can be used as dust proxies at ODP 1208 (Kienast et al., 2016; Patterson et al., 1999; Serno et al., 2014). Using these specific indicators of dust along with knowledge about their sources, we also provide a new estimate of dust fractions and fluxes that adjusts these previous records for potential volcanic ash input. Overall, our findings highlight the importance of accurate reconstructions of windblown sediment for determining dust production and transport mechanisms, the timing and effects of arid-region landscape evolution, and the potential limitations of interpreting certain paleo-dust proxies obtained from the North Pacific Ocean and CLP.

2. Material and Methods

2.1. Core Location and Age Models

ODP Leg 198 site 1208 (36.1°N, 158.2°E, 3,345.7 m water depth) was cored on the Shatsky Rise in the western North Pacific (Bralower et al., 2002). It was previously suggested that the late Neogene to core-top section of ODP 1208 could be a drift deposit (Bralower et al., 2002), or at a minimum experienced some amount of sediment redistribution (Gylesjö, 2005), although subsequent work challenges these earlier findings (W. Zhang et al., 2016). In either case, the use of two CFPs in these records allows us to account for sediment focusing/winnowing that is present and determine an accurate reconstruction of dust fluxes to the site.

To construct the late Quaternary age model for site 1208, 204 samples of approximately 1–4 shells of *Uviergina* spp. ($n = 194$) or *Cibicidoides wuellerstorfi* ($n = 10$) were picked from the >250 μm size fraction and run for stable isotopes. Samples were analyzed on an Elementar Isoprime 100 stable isotope ratio mass spectrometer with dual inlet at Lamont-Doherty Earth Observatory (Palisades, New York, USA) with a long-term precision of ±0.06‰. A species correction (+0.64‰) was applied to the oxygen isotope data from *C. wuellerstorfi*. An age model was constructed by combining previously published benthic δ^{18}O values (Ford & Raymo, 2020; Woodard et al., 2014) with the data generated here and using HMM-Stack Matlab code (Butcher et al., 2017; Lin et al., 2014) which

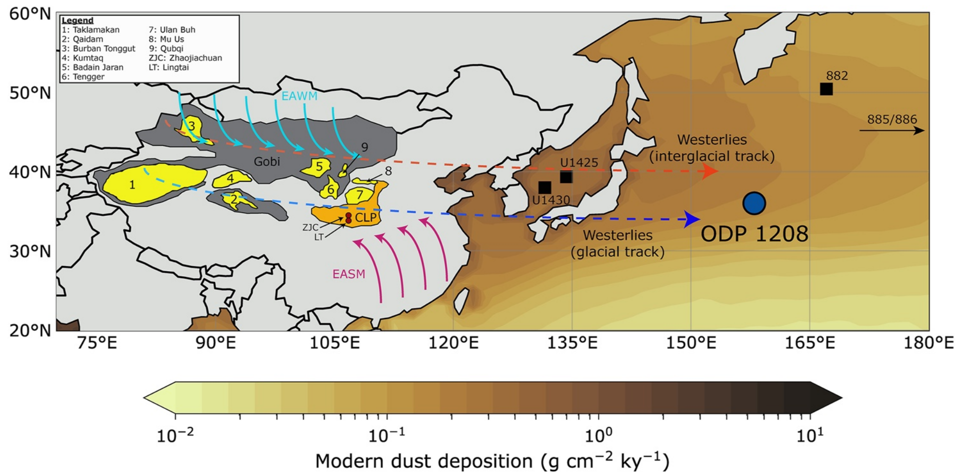

Figure 1. Map of major features relevant to East Asian dust dynamics with modeled modern dust deposition rates for the North Pacific (Albani et al., 2014). Blue circle represents the location of ODP 1208, while black squares and arrows indicate approximate positions of other core sites relevant to this study. Yellow regions on land represent sandy deserts. Dark gray regions indicate stony (Gobi) deserts. Light blue arrows indicate winds from the East Asian winter monsoon. Purple arrows represent direction of winds and moisture transport from the East Asian summer monsoon. Red and dark blue arrows qualitatively indicate the dominant position of the westerly winds during interglacial and glacial periods of the Quaternary, respectively (Abell et al., 2021; Kapp et al., 2011).

aligns the $\delta^{18}O$ values to Prob-stack (Figure S1 in Supporting Information S1) (Ahn et al., 2017). Additionally, core gaps in the single-core site ODP 1208 necessitated using several tie points (Figure S1 in Supporting Information S1). For the late Pliocene-early Pleistocene, we use the age model of Venti and Billups (2012), which is derived from a benthic $\delta^{18}O$ record tuned to the LR04 benthic stack (Lisiecki & Raymo, 2005).

Cutoff times for glacial-interglacial boundaries used in the determination of dust flux averages are based on the LR04 global benthic oxygen isotope stack (Lisiecki & Raymo, 2005), unless a peak in dust is the first or last sample within an interglacial, at which point it remains in the nearest glacial. We attribute these offsets to minor differences between the global composite and the core-specific age models. The data taken from Abell et al. (2021) was specifically selected so that the oldest sample begins with the first available helium isotope datapoint prior to the intensification of Northern Hemisphere Glaciation at ~2,730 ka.

2.2. Th and He Isotope Data

All ODP 1208 Th and He isotope data used in this study have been published or are available from data repositories (Abell et al., 2021; Kinsley, 2019; Kinsley et al., 2022; McGee et al., 2016). Details on isotope measurements are available in the original studies. All uncertainties for the Th isotope data from Kinsley (2019) and Kinsley et al. (2022) are the same as those reported in the original publication and data set. We have updated the uncertainties on ^{232}Th-derived dust fractions and fluxes from Abell et al. (2021) to reflect the uncertainty on the endmember value (14 ± 1 ppm) and to align with the approach of Kinsley (2019) and Kinsley et al. (2022). Averaging of He isotope replicates from both Abell et al. (2021) and McGee et al. (2016) is performed after replicate-specific extraterrestrial ^{3}He ($^3He_{ET}$) and terrestrial ^{4}He ($^4He_{terr}$) concentrations are determined. Finally, as with ^{232}Th, uncertainties related to $^4He_{terr}$-derived dust concentrations and fluxes have been adjusted to reflect endmember uncertainty (1,855 ± 715 ncc g^{-1}) (Abell et al., 2021; McGee et al., 2016).

2.3. Calcium Carbonate and Opal Data

We measured calcium carbonate ($CaCO_3$) concentrations for the late Pliocene-early Pleistocene sediments ($N = 58$) at ODP 1208. Samples were homogenized, weighed, and acidified with phosphoric acid prior to analysis on a CM5012 CO_2 Coulometer at Lamont-Doherty Earth Observatory. We derived an uncertainty of 0.93% [1σ] based on the reproducibility of a pure carbonate standard. Opal data for this same time interval is from Abell et al. (2021). For the late Pleistocene-Holocen section, all $CaCO_3$ and opal concentrations are from Kinsley et al. (2022) and were produced following similar methods to the data produced here and in Abell et al. (2021).

2.4. Determination of Dust Concentrations

To constrain the dust component of ODP 1208 Plio-Pleistocene sediments, we apply two separate approaches, both of which use ^{232}Th concentrations as the dust proxy. The application of ^{232}Th as a proxy for wind-blown dust has been extensively utilized in previous geochemical studies (see Kienast et al., 2016; McGee et al., 2016).

First, we follow the same methodology of the original studies (Abell et al., 2021; Kinsley, 2019; Kinsley et al., 2022) and assume all ^{232}Th is derived from dust ($^{232}Th_{total}$). This assumption is supported by geochemical data presented in Zhang et al. (2016), who suggest low Th concentrations in the non-dust lithogenic component of ODP 1208 sediments. Dust fractions are then determined by dividing the measured ^{232}Th concentrations in the sediments by the average ^{232}Th concentration of fine-grained dust from Asia (14 ± 1 ppm; McGee et al., 2016).

In the second approach, we attempt to provide a more conservative estimate of dust by accounting for potentially variable volcanic contributions to the measured ^{232}Th concentrations in both time intervals. The lithogenic fraction of open-ocean, mid-latitude North Pacific sediments can consist of both dust and volcanic material (Olivarez et al., 1991), which could confound dust concentrations determined via elemental/isotopic signatures. Specifically, low-resolution trace element and radiogenic isotope endmember modeling from ODP 1208 sediments spanning the last ∼25 My suggests volcanic ash comprises ∼10%–25% of the terrigenous fraction in the Plio-Pleistocene, although one sample does show a higher (∼45%) value (W. Zhang et al., 2016). At the nearby site of ODP 1209 (∼400 km away), volcanic ash contributions for the last ∼450 ky have been modeled using grain size distributions (W. Zhang et al., 2020). As with ODP 1208, the volcanic contribution is estimated to be between ∼0 and 40% (aside from a single datapoint). Finally, using core-top geochemical data from the western North Pacific, Serno et al. (2014) determined the non-dust lithogenic fraction of sediments in this region to be anywhere from ∼0% to 65%. Considering these findings, and evidence that volcanic material derived from Japan and the Korean Peninsula contains Th at concentrations ranging from ∼<1 ppm to >23 ppm (Anderson et al., 2020; Masuda & Aoki, 1979; Sakuyama & Nesbitt, 1986; Takahashi et al., 2012), we follow the methodology of Serno et al. (2014) to calculate dust fractions and dust fluxes based on adjusted ^{232}Th concentrations ($^{232}Th_{adj}$). Briefly, total lithogenic fractions are determined via subtraction of $CaCO_3$ and opal concentrations, which are then used to produce lithogenic ^{232}Th ($^{232}Th_{lith}$) and $^4He_{terr}$ ($^4He_{terr\ lith}$) values. Utilizing these and previously published data, a volcanic endmember for ^{232}Th ($^{232}Th_{volc}$) is constrained (a value of ∼5.65 ppm is used here), which is then applied to derive adjusted (i.e., corrected for volcanic input) dust fractions ($Dust_{Th\ adj}$) and dust fluxes (Dust $flux_{Th\ adj}$) for both dust data sets. Further details and equations related to this methodology can be found in Text S1 of the Supporting Information S1.

2.5. Determination of $^3He_{ET}$ and $^4He_{terr}$ Concentrations

The concentration of $^3He_{ET}$ in samples from Abell et al. (2021), and those determined here for the six samples from McGee et al. (2016), were calculated through a mixing equation using measured ^{3}He concentrations and $^3He/^4He$ ratios (Marcantonio et al., 1995):

$$[^3He_{ET}] = [^3He_{meas}] * ((1 - (^3He/^4He)_{terr}/(^3He/^4He)_{meas})/(1 - (^3He/^4He)_{terr}/(^3He/^4He)_{ET})) \quad (1)$$

where $(^3He/^4He)_{terr}$ and $(^3He/^4He)_{ET}$ are the helium isotope ratios of the assumed terrigenous and extraterrestrial endmembers, respectively. A similar approach was applied to determine the concentration of $^4He_{terr}$ (Patterson et al., 1999; Winckler et al., 2005):

$$[^4He_{terr}] = [^4He_{meas}] * (((^3He/^4He)_{meas} - (^3He/^4He)_{ET})/((^3He/^4He)_{terr} - (^3He/^4He)_{ET})) \quad (2)$$

Following Abell et al. (2021) and McGee et al. (2016), along with several previous studies (Middleton et al., 2016, 2018; Winckler et al., 2005), values of 2.4×10^{-4} (Nier & Schlutter, 1992) and 2×10^{-8} (Ozima & Podosek, 1983) were used for $(^3He/^4He)_{ET}$ and $(^3He/^4He)_{terr}$, respectively. Because the choice of these endmembers can substantially influence the calculated $[^3He_{ET}]$ of the samples, we analyze the sensitivity of the He isotope data to the $(^3He/^4He)_{terr}$ endmember in Text S2 of the Supporting Information S1. We find that within a reasonable range of endmembers, our results are not substantially affected.

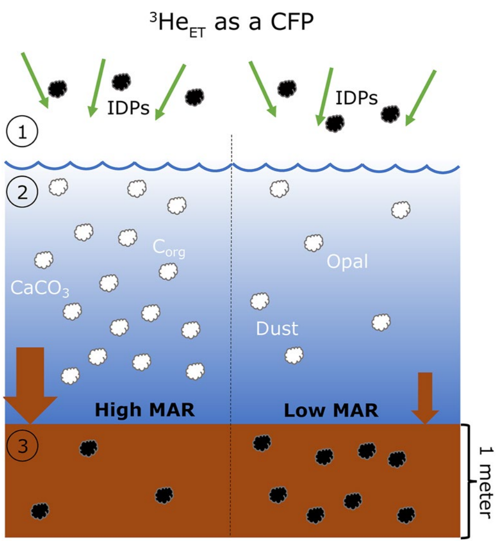

Figure 2. Schematic of the fundamental principles and assumptions related to the use of the CFP $^3He_{ET}$. (1) Interplanetary dust particles (IDPs) fall to Earth at an assumed near-constant rate through the time interval of interest. This "space dust" is the carrier phase of $^3He_{ET}$ and falls into the ocean after traveling through the atmosphere. (2) The IDPs, along with biogenic (e.g., $CaCO_3$, opal, and organic carbon (C_{org})) and terrigenous material (e.g., dust, volcanic material, riverine sediments, and ice-rafted detritus) produced in or delivered to the ocean, fall to the seafloor. If more material falls in a given time interval, this will produce a higher vertical sediment mass accumulation rate (MAR), and vice versa. (3) In a given depth of sediment, the concentration of $^3He_{ET}$ would be lower if sediment accumulates rapidly than if it accumulated more slowly. This is because the IDPs are being diluted by other material. It is this dilution, and the assumed constant flux, that allow for the determination of vertical sediment MARs.

2.6. $^3He_{ET}$ and Initial Excess ^{230}Th ($^{230}Th_{0xs}$) as Constant Flux Proxies

CFPs, such as $^{230}Th_{0xs}$, which is produced in the water column via the decay of uranium, and $^3He_{ET}$, which is delivered to Earth in interplanetary dust particles, can provide vertical MARs of seafloor sediments via the equation:

$$\mathrm{MAR} = \frac{F_{CFP}}{[CFP]} \tag{3}$$

where F_{CFP} is the flux of the CFP to the sediments and [CFP] is the concentration of the CFP in the sediment sample (see Figure 2 for a schematic of this process for $^3He_{ET}$) (Costa et al., 2020; McGee & Mukhopadhyay, 2013). The basic premise behind these proxies is that they fall to the sediment at a relatively constant rate, and their concentration in the sediments is only affected by dilution from other sediment constituents and decay (relevant for ^{230}Th). Assuming that any sediment focused or winnowed near the site contains similar concentrations of $^3He_{ET}$ or $^{230}Th_{0xs}$ as contemporaneous sediments settling down from directly above the site, these CFPs can be utilized to determine the vertical MAR of various sedimentary constituents through time (Costa et al., 2020; McGee & Mukhopadhyay, 2013).

2.7. Efficacy of the CFP $^3He_{ET}$ at ODP 1208

The use of CFPs relies on the assumption that the flux of the proxy to the sediments is constant over the period of interest. The availability of both $^{230}Th_{0xs}$ and $^3He_{ET}$ data at ODP 1208 for the past ~20 ky allows us to test the efficacy of $^3He_{ET}$ and determine the $^3He_{ET}$ flux using the $^{230}Th_{0xs}$-normalized MAR. $^3He_{ET}$ fluxes remain relatively constant and produce an average consistent with the late Quaternary value (~0.74 ± 0.21 [1σ] vs. 0.8 ± 0.3 [1σ] pcc cm^{-2} ky^{-1}) (Figure 3a) (McGee & Mukhopadhyay, 2013), providing support for the proxy's viability at this site. We also present these results as a comparison of MARs derived using both approaches (Figure 3b) (Kinsley, 2019; Kinsley et al., 2022; McGee et al., 2016). Overall, we provide evidence that the CFP $^3He_{ET}$ can be reliably applied at ODP 1208.

2.8. Calculation of Uncertainties for $^3He_{ET}$-Derived Fluxes

Errors estimates associated with $^3He_{ET}$-derived fluxes consist of analytical uncertainties for $^3He_{ET}$ concentrations, statistical uncertainties associated with $^3He_{ET}$ in marine sediments (Farley et al., 1997; Patterson & Farley, 1998), and the uncertainty on the late Quaternary value of F_{3HeET} (McGee & Mukhopadhyay, 2013), all propagated to produce a final 1σ uncertainty. We utilize the same uncertainties as provided in Abell et al. (2021) for the late Pliocene-early Pleistocene data set and follow the same approach of Abell et al. (2021) for the $^3He_{ET}$ data of McGee et al. (2016).

3. Results

3.1. North Pacific Plio-Pleistocene Dust Fluxes

First, we present total ^{232}Th ($^{232}Th_{total}$)-derived dust fluxes for the last ~330 ky (Kinsley, 2019; Kinsley et al., 2022) and the interval spanning ~2,500–2,730 ka (Abell et al., 2021) that are based on the CFPs $^{230}Th_{0xs}$ and $^3He_{ET}$, respectively (see Section 2). Because we seek to constrain only the East Asian dust fraction of terrigenous sediments at ODP 1208, we then provide the same set of values for dust fluxes based on ^{232}Th concentrations corrected for potential volcanic input (Dust flux$_{Th\ adj}$; see Section 2 and Text S1 in Supporting Information S1) and compare the results from both approaches (Table 1 and Figure 4).

In the late Pleistocene-Holocene, where data are available for marine isotope stages (MIS) 1–3, a portion of MIS 4 and 5 (a core gap likely leads to the missing sediment between ~67 and 115 ka; see Figure S1 in Supporting Information S1 and age model description in Section 2), and MIS 6–9, the glacial and interglacial dust flux

10.1029/2022PA004571

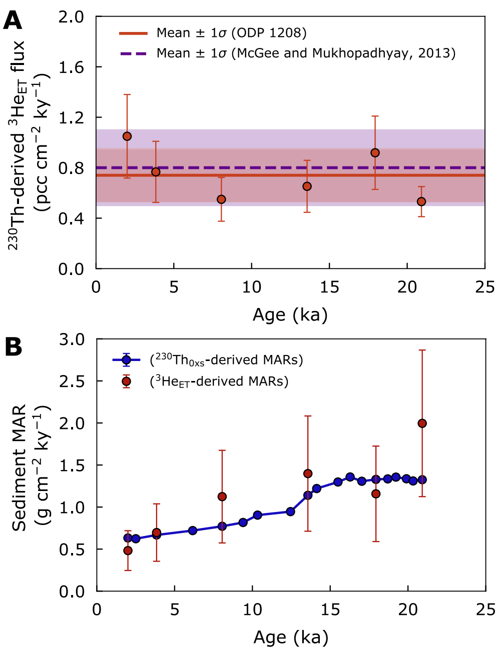

Figure 3. Late Quaternary $^{230}Th_{0xs}$ and $^{3}He_{ET}$ data for ODP 1208. (a) $^{230}Th_{0xs}$-derived $^{3}He_{ET}$ fluxes for the last ~20 ky. Red circles are determined using $^{230}Th_{0xs}$ (Kinsley, 2019; Kinsley et al., 2022) and $^{3}He_{ET}$ concentrations that were calculated from ^{4}He concentrations and $^{3}He/^{4}He$ ratios provided in McGee et al. (2016). Error bars include analytical uncertainties on all isotopes, as well as the statistical uncertainty related to $^{3}He_{ET}$, the value of which is derived from Abell et al. (2021). The dark red line is the average of the six points, and the red shaded region is the associated 1σ uncertainty. The dark purple line is the global average of the late Quaternary flux of $^{3}He_{ET}$, and the purple shaded region is the associated 1σ uncertainty (McGee & Mukhopadhyay, 2013). (b) Late Quaternary CFP-derived sediment mass accumulation rates for ODP 1208. The data in purple are based on $^{230}Th_{0xs}$ (Kinsley, 2019; Kinsley et al., 2022). Error bars incorporate all propagated uncertainties. The data in red are based on $^{3}He_{ET}$-derived fluxes. Error bars include analytical uncertainties for $^{3}He_{ET}$, the statistical uncertainty related to $^{3}He_{ET}$ using the value from Abell et al. (2021), as well as the uncertainty related to the constant flux of $^{3}He_{ET}$ in the late Quaternary (McGee & Mukhopadhyay, 2013).

averages at ODP 1208 are ~0.49 ± 0.13 [1σ] g cm^{-2} ky^{-1} and ~0.38 ± 0.15 [1σ] g cm^{-2} ky^{-1} respectively, while the mean glacial maximum and interglacial minimum values are ~0.71 ± 0.06 [1σ] g cm^{-2} ky^{-1} and ~0.23 ± 0.11 [1σ] g cm^{-2} ky^{-1}, respectively (Table 1). Late Pliocene-early Pleistocene glacial dust fluxes during MIS G6, G4, G2, 104, and 100 average ~1.14 ± 0.50 [1σ] g cm^{-2} ky^{-1} while the mean of the corresponding seven interglacials (MIS G7-101) is ~0.55 ± 0.26 [1σ] g cm^{-2} ky^{-1} (Table 1). Additionally, the average maximum dust flux following the intensification of Northern Hemisphere Glaciation for glacials is ~1.69 ± 0.65 [1σ] g cm^{-2} ky^{-1}, while the mean interglacial minimum is ~0.48 ± 0.22 [1σ] g cm^{-2} ka^{-1}. Late Pliocene-early Pleistocene glacials thus experienced an average of ~2.3 times greater dust deposition than late Pleistocene glacials, whereas interglacials received ~1.5 times more dust during the ~2,500–2,730 ka interval. Finally, we find that the relative increase from average interglacial minima to glacial maxima is greater in the late Pliocene-early Pleistocene than the late Pleistocene (~3.5 times compared to ~3.0 times), as is the average glacial to interglacial dust flux (~2.1 times compared to ~1.3 times).

Dust fractions based on $^{232}Th_{adj}$ suggest volcanic ash (assuming a two-component detrital fraction) may, on average, comprise upwards of ~45% and ~40% of the total lithogenic material in late Pliocene-early Pleistocene and late Pleistocene-Holocene sediments at ODP 1208, respectively, which is consistent with previous work in the region (Serno et al., 2014; W. Zhang et al., 2016, 2020). When applying a ^{232}Th correction for volcanic detritus in the sediments (see Section 2 as well as Text S1 in Supporting Information S1), average late Pleistocene glacial and interglacial dust fluxes are ~0.39 ± 0.11 [1σ] g cm^{-2} ky^{-1} and ~0.29 ± 0.13 [1σ] g cm^{-2} ky^{-1}, respectively, while the mean glacial maximum and interglacial minimum are ~0.58 ± 0.06 [1σ] g cm^{-2} ky^{-1} and ~0.17 ± 0.09 [1σ] g cm^{-2} ky^{-1}, respectively (Table 1 and Figure 4a). The corresponding values for the late Pliocene-early Pleistocene are ~0.88 ± 0.42 [1σ] g cm^{-2} ky^{-1}, ~0.37 ± 0.20 [1σ] g cm^{-2} ky^{-1}, ~1.30 ± 0.53 [1σ] g cm^{-2} ky^{-1}, and ~0.28 ± 0.14 [1σ] g cm^{-2} ky^{-1}, respectively (Table 1 and Figure 4b). Correcting for the presence of volcanic ash decreases the ratios of early to late Quaternary glacial and interglacial dust fluxes marginally from ~2.3 to 2.2 times and ~1.5 to 1.3 times, respectively. Opposingly, the correction leads to mean late Pliocene-early Pleistocene glacial dust fluxes ~2.4 times greater than interglacial fluxes, and this value is ~1.4 times for the late Pleistocene.

Considering the uncertainties and assumptions associated with each methodology of dust flux determination (see Text S1 in Supporting Information S1), and to be consistent with the original studies, we utilize the $^{232}Th_{total}$-derived dust fluxes for the remainder of the discussion (Figure 5). Importantly, we note that our conclusions are relevant to both data sets (Table 1). Keeping the substantial uncertainties related to the CFP-derived dust fluxes in mind, particularly in the late Pliocene-early Pleistocene, we focus our discussion around changing glacial dust fluxes (and the variable glacial-interglacial dust flux variability brought about by the glacial dust fluxes).

3.2. $^{4}He_{terr}/^{232}Th$ Ratios

While both $^{4}He_{terr}$ and ^{232}Th can serve as individual dust proxies (e.g., Kienast et al., 2016; Patterson et al., 1999), as evidenced by their consistency during the late Pleistocene-Holocene (Figure S2 in Supporting Information S1) and late Pliocene-early Pleistocene (Abell et al., 2021), their absolute abundance in marine sediments can be influenced by a variety of factors. These include the presence of volcanic material (hence their utilization here to determine volcanic contributions), as well as the grain size and provenance of the dust they comprise (McGee et al., 2016; Patterson et al., 1999; Serno et al., 2014). Specifically, $^{4}He_{terr}$ is negligible in volcanics (Patterson et al., 1999), while ^{232}Th concentrations can vary widely between dust and ash (Anderson et al., 2020; Dunlea et al., 2015; McGee et al., 2016; Sakuyama & Nesbitt, 1986; Takahashi et al., 2012). In addition, sediment grain size affects the

Table 1
Comparison of ODP 1208 Late Pleistocene-Holocene (LP) and Late Pliocene-Early Pleistocene (EP) Glacial-Interglacial Dust Fluxes (g cm^{-2} ky^{-1})

	Glacial	Interglacial	G/IG ratio	Glacial maxima	Interglacial minima	G-max/IG-min ratio
Total ^{232}Th-derived dust fluxes						
LP						
Average	0.49	0.38	1.31	0.71	0.23	3.03
Median	0.50	0.38	1.33	0.72	0.22	3.29
1σ	0.13	0.15		0.06	0.11	
EP						
Average	1.14	0.55	2.08	1.69	0.48	3.53
Median	1.05	0.44	2.40	1.49	0.44	3.41
1σ	0.50	0.26		0.65	0.22	
EP[a]						
Average	1.08	0.55	1.96	1.50	0.48	3.15
Median	0.99	0.44	2.28	1.32	0.44	3.04
1σ	0.51	0.26		0.74	0.22	
Volcanic ash adjusted ^{232}Th-derived dust fluxes						
LP						
Average	0.39	0.29	1.36	0.58	0.17	3.38
Median	0.40	0.29	1.41	0.61	0.15	4.11
1σ	0.11	0.13		0.06	0.09	
EP						
Average	0.88	0.37	2.38	1.30	0.28	4.58
Median	0.79	0.30	2.63	1.16	0.26	4.46
1σ	0.42	0.20		0.53	0.14	
EP[a]						
Average	0.83	0.37	2.26	1.16	0.28	4.09
Median	0.77	0.30	2.58	1.05	0.26	4.03
1σ	0.42	0.20		0.58	0.14	

[a]While MIS 102 is not considered in the results due to a lack of a dust peak during the interval, we do provide revised dust fluxes and ratios here which include MIS 102.

concentration of the two isotopes in opposite directions, with smaller grains containing less $^{4}He_{terr}$ but more ^{232}Th than larger grains (McGee et al., 2016). Finally, the source regions of dust may have distinct geochemistry. Considering all this evidence, the ratio of the two isotopes ($^{4}He_{terr}/^{232}Th_{total}$) could be exploited to provide qualitative information about these potential contributors, and thus aid in our analysis of changing dust dynamics over the Quaternary.

At ODP 1208, the number of available samples that contain data for both proxies are sparse in the late Pleistocene-Holocene, but the ratio does vary, with a minimum value of 96 ncc μg^{-1} during the Holocene and a maximum of 136 ncc μg^{-1} during the Last Glacial Maximum (Figure 6a). The variability in the $^{4}He_{terr}/^{232}Th_{total}$ ratio is greater during the late Pliocene-early Pleistocene (Figure 6b), ranging from 51 to 161 ncc μg^{-1}.

4. Discussion

4.1. A New Marine Perspective on Dust From Eastern Asia

Our work provides the first comparison of high-resolution, CFP-derived dust fluxes from the earliest glacial-interglacial cycles after the inception of major Northern Hemisphere ice sheets to those determined for the late Quaternary from an area downwind of the arid regions of East Asia. The methodologies applied in these records, previous work on the core, and the site location itself offer numerous advantages for reconstructing dust production in eastern Asia using

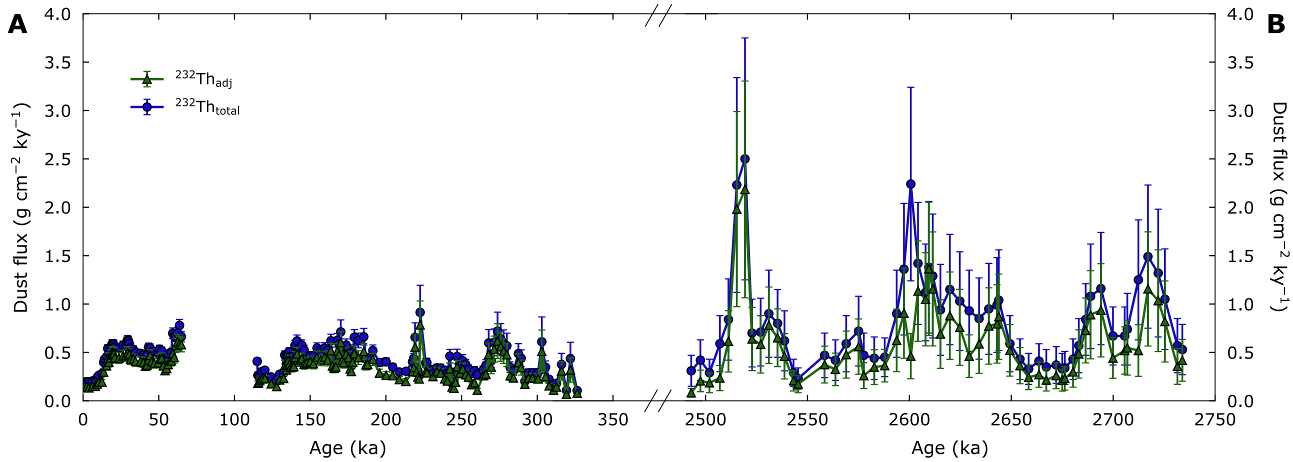

Figure 4. ^{232}Th$_{total}$- and ^{232}Th$_{adj}$-derived dust fluxes from ODP 1208. (a) Late Pleistocene-Holocene dust fluxes determined using both ^{232}Th$_{total}$ dust concentrations (purple line) (Kinsley, 2019; Kinsley et al., 2022) and ^{232}Th$_{adj}$ dust (green line). (b) Same as (a), but for the late Pliocene-early Pleistocene (Abell et al., 2021). Error bars incorporate all propagated uncertainty related to the determination of dust fluxes for each individual method.

marine sediments. In terms of age control, ODP 1208 benefits from having two high-resolution age models based on oxygen isotopes for the intervals of the Quaternary where CFP-derived dust flux data exists (This study; Venti & Billups, 2012). Additionally, the core, located at ∼36°N and >1,500 km from the coast of Japan, lies in the path of dust plumes emanating from East Asian deserts (Uno et al., 2009) and is remote enough from land that detrital input from rivers and ice-rafted debris is minimal (McCarron et al., 2020). The other possible terrigenous component present at ODP 1208 is volcanic material, which could complicate dust reconstructions. However, the application of multiple elemental and isotopic proxies for dust, along with previously published geochemical results, allows us to estimate the impact of volcanic detritus on ^{232}Th-derived dust fluxes during the Plio-Pleistocene (see Section 2 as well as Text S1 in Supporting Information S1) (Abell et al., 2021; Kinsley, 2019; Kinsley et al., 2022; McGee et al., 2016; Serno et al., 2014; W. Zhang et al., 2016, 2020). Finally, while we have previously noted that ^{232}Th concentrations can also be impacted by changing dust sources and sediment grain size, the interquartile variability in ^{232}Th content across several East Asian dust sources in the grain size fraction expected to reach ODP 1208 cannot fully explain our average two-fold decrease in glacial dust fluxes across the Quaternary (McGee et al., 2016).

Our finding that glacial dust fluxes decreased and interglacial dust fluxes likely remained relatively stable at ODP 1208 from the early to late Quaternary is at odds with the limited other dust accumulation rates from the

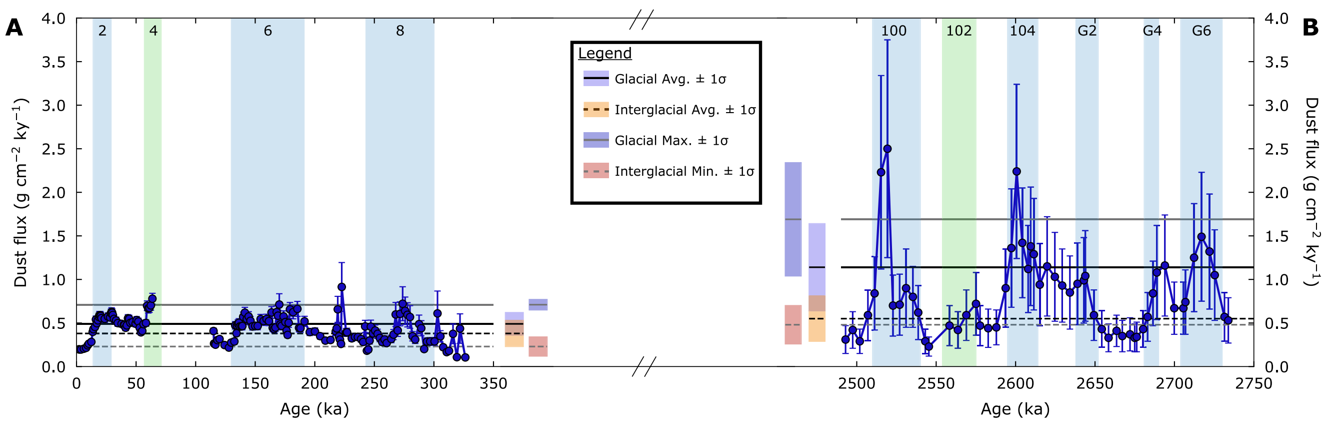

Figure 5. North Pacific dust fluxes from ODP 1208. (a) Late Pleistocene-Holocene dust fluxes determined using ^{232}Th$_{total}$ concentrations and ^{230}Th$_{xs0}$-derived sediment rain rates (Kinsley, 2019; Kinsley et al., 2022). Error bars represent all propagated uncertainties for both isotopes. (b) Late Pliocene-early Pleistocene dust fluxes determined using ^{232}Th concentrations and ^{3}He$_{ET}$-derived sediment rain rates (Abell et al., 2021). Error bars represent all propagated analytical uncertainties for both isotopes along with statistical and systematic uncertainties associated with ^{3}He$_{ET}$. Blue bars and the corresponding MIS numbers represent glacial intervals used in the calculation of dust flux averages. Green bars represent MIS 4 and 102, where either data does not cover the entire interval (MIS 4) or no peaks in dust are present (MIS 102). We do not include values from MIS 102 in our primary calculations, but values incorporating this interval are included in Table 1.

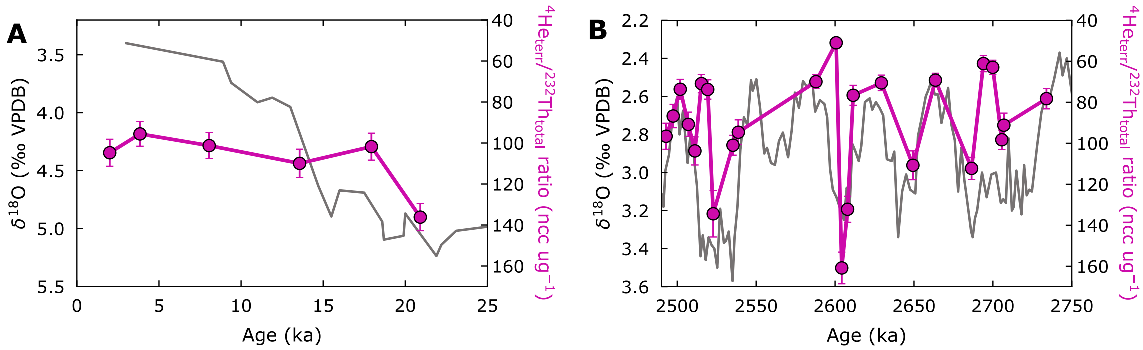

Figure 6. He and Th isotope ratios. (a) $^{4}He_{terr}/^{232}Th_{total}$ ratios for the late Pleistocene-Holocene. (b) Same as (a), but for the late Pliocene-early Pleistocene. The benthic oxygen isotope records shown are from this study (a) and Venti and Billups (2012) (b). Data used to calculate the ratios is from McGee et al. (2016), Kinsley et al. (2022), Kinsley (2019), and Abell et al. (2021). Error bars represent the full propagated uncertainty for both isotopes.

Sea of Japan and North Pacific Ocean (Figure 7) (Anderson et al., 2020; Haug et al., 1995; Lee et al., 2022; Rea et al., 1998; W. Zhang et al., 2016; Q. Zhang et al., 2020a). Importantly, many of the previously published data sets from other sites also display substantial differences from each other, possibly highlighting the limitations of those data sets. For ease of comparison, we calculate dust amplification factors for all records mentioned here by dividing the core-specific dust fluxes at each point by the core-specific average dust MAR for the interval from ~0 to 2,730 ka. As such, all values greater than 1 indicate higher dust fluxes than the average for the period shown, and values less than 1 represent lower dust fluxes than the average.

There are several reasons why each of these records diverge from one another. Many of these revolve around complications that suggest some records may be problematic if used to reconstruct a purely regional dust signal from East Asia in the Pleistocene. Of the available records presented here, all are based on age model-derived sediment accumulation rates, which can be affected by lateral sediment advection (Costa et al., 2020). There is evidence suggesting lateral sediment advection occurred during various intervals of time at ODP 882 (Serno et al., 2017), IODP U1430 (Anderson et al., 2020), and ODP 885/886 (Abell et al., 2021; Bridges et al., 2021). Due to the nature of both near-surface and deep currents in the Sea of Japan, sites located in this region could be particularly susceptible to sediment redistribution (Hase et al., 1999; Kim et al., 2008; Trusenkova & Ishida, 2005). In addition, many of these sites likely experienced input from lithogenic sources aside from wind-blown dust during the Quaternary, such as ice-rafted debris (ODP 882; Haug et al., 1999; McCarron et al., 2020), volcanic material (ODP 885/886, IODP U1430, and IODP U1425; Anderson et al., 2020; Bailey et al., 2011; Lee et al., 2022; Q. Zhang et al., 2020a), —this could be accounted for if specific methods are applied (e.g., Anderson et al., 2020; Lee et al., 2022; Serno et al., 2014; Q. Zhang et al., 2020a)—and riverine input (IODP U1430 and IODP U1425; Anderson et al., 2020; Gallagher et al., 2015; Lee et al., 2022; Shen et al., 2017).

Finally, we note that while the age model-derived, operationally defined eolian flux from Zhang et al. (2016) at ODP 1208 shows declining overall fluxes through the Quaternary (consistent with our new CFP-derived dust flux reconstruction at the site), this pattern needs to be carefully reassessed in the framework of higher-resolution age models. Specifically, Zhang et al. (2016) use a low-resolution age model based on shipboard data (Bralower et al., 2002) to calculate sedimentations rates, and in turn dust fluxes for the Quaternary. However, a much higher-resolution age model exists for part of the Pleistocene and Pliocene (Venti & Billups, 2012), and now, combined with existing data from Woodard et al. (2014) and Ford and Raymo (2020), we have an additional high-resolution age model for the late Quaternary. One way to evaluate the pattern observed by Zhang et al. (2016) for the Quaternary at ODP 1208 is to use these two higher-resolution age models, shipboard dry bulk densities, and our $^{232}Th_{total}$ concentration data to produce age model-derived dust fluxes for our two intervals of time (Figure S3 in Supporting Information S1). Zhang et al. (2016), using Q-model factor analysis of trace element concentrations, suggested that Th in ODP 1208 is predominantly from dust and not volcanic ash, and as such our ^{232}Th concentrations should serve as an acceptable approximation of the operationally defined eolian fraction in their study (at least for this example). We find that, if a higher-resolution age model is used to produce linear sedimentation rates, glacial dust fluxes increase from the early Quaternary to the late Quaternary. This again supports our argument for the utility of CFPs, and our conclusion that the available data sets of dust fluxes from the Sea of Japan and North Pacific are inconsistent.

10.1029/2022PA004571

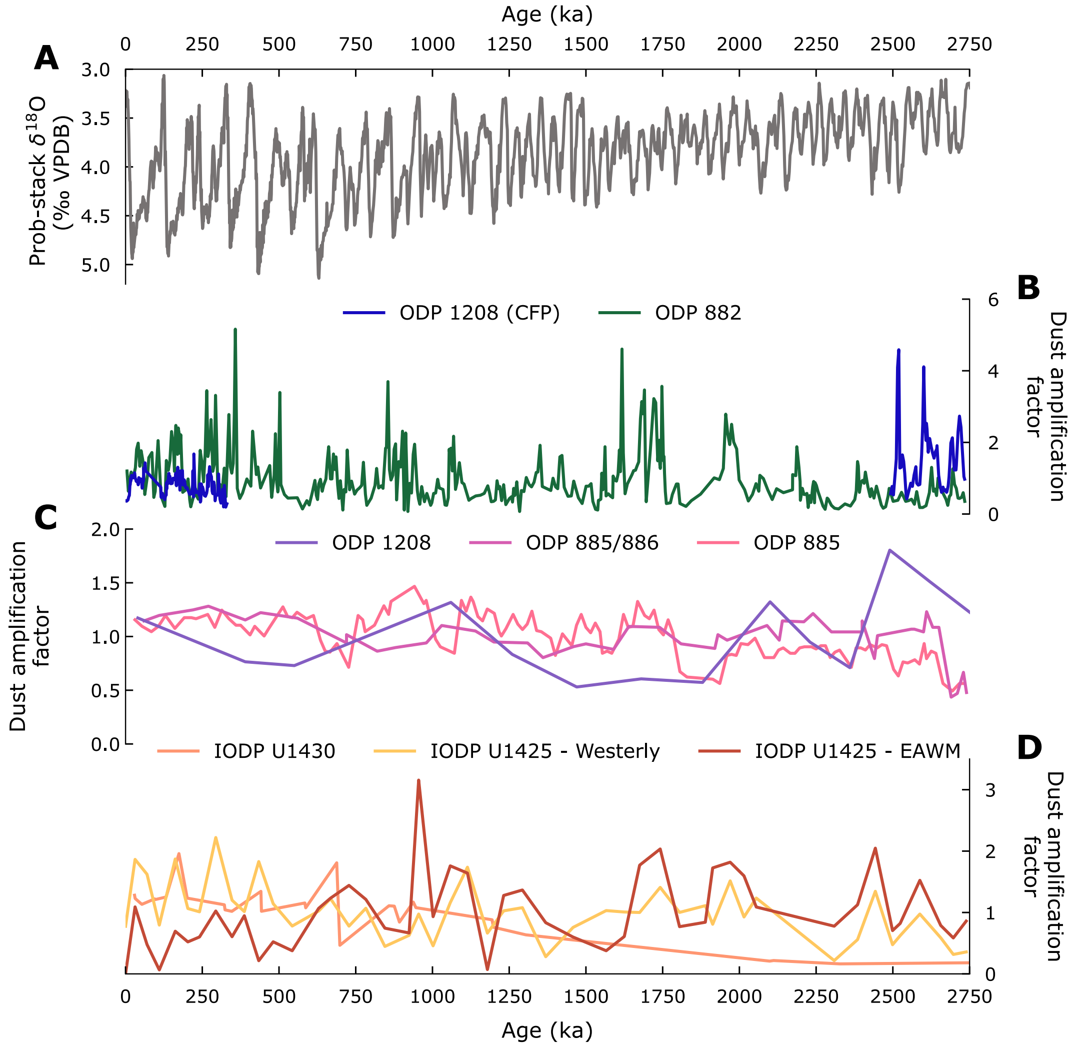

Figure 7. Quaternary evolution of dust fluxes from various marine sediment cores downwind of East Asia. (a) Prob-stack benthic oxygen isotope stack (Ahn et al., 2017). (b) High-resolution Quaternary dust amplification factors from the North Pacific for ODP 1208 (based on $^{232}Th_{total}$ dust fluxes) (Abell et al., 2021; Kinsley, 2019; Kinsley et al., 2022) and ODP 882 (Haug et al., 1995). (c) Low-resolution Quaternary dust amplification factors from the North Pacific for ODP 1208 (W. Zhang et al., 2016), ODP 885 (Q. Zhang et al., 2020a), and ODP 885/886 (Rea et al., 1998). (d) Low-resolution Quaternary dust amplification factors from the Sea of Japan for IODP U1430 (Anderson et al., 2020), the "Westerly" component of dust for IODP U1425 (Lee et al., 2022), and the "East Asian Winter Monsoon" (EAWM) component of dust for IODP U1425 (Lee et al., 2022).

While we do not propose that each of these other dust flux records are invalidated by contributions of material aside from vertically delivered East Asian dust, considering the uncertainty stemming from these complicating factors, we suggest that our combined CFP-derived dust flux records may be valuable for accurately describing Pleistocene East Asian dust dynamics, at least from a mid-latitude North Pacific perspective. We now offer several possible explanations for the observed decreasing glacial dust flux trend and glacial-interglacial variability present in ODP 1208 dust fluxes that we anticipate will serve as guides for future work attempting to interpret existing incongruities between Quaternary North Pacific dust records.

4.2. Landscape Evolution as a Mechanism for Decreasing Glacial East Asian Dust Emissions Through the Quaternary

The elevated absolute glacial dust fluxes and glacial-interglacial dust flux variability during the late Pliocene-early Pleistocene compared to the late Pleistocene at ODP 1208 also differ profoundly from other global records of dust

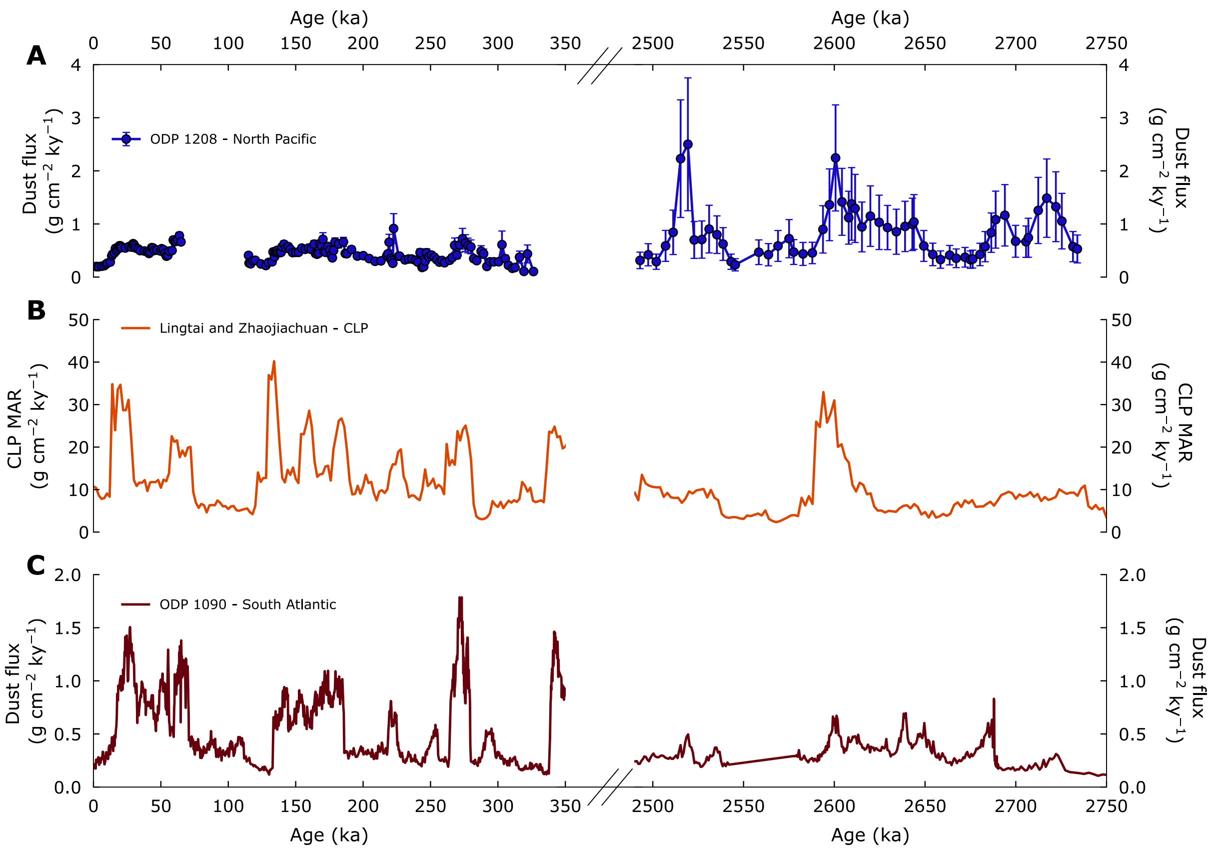

Figure 8. Comparison of early and late Quaternary dust fluxes from various archives. (a) Dust fluxes from ODP 1208 in the North Pacific (based on $^{232}Th_{total}$ concentrations) (Abell et al., 2021; Kinsley, 2019; Kinsley et al., 2022). Error bars represent propagated analytical uncertainties for both $^{232}Th_{total}$ and $^{230}Th_{0xs}$ for the late Quaternary, and error bars represent propagated analytical uncertainties on Th_{total} and $^{3}He_{ET}$ concentrations, statistical uncertainties associated with $^{3}He_{ET}$, and uncertainty on the constant flux of $^{3}He_{ET}$ for the early Quaternary. (b) Sediment mass accumulation rates for the CLP (Y. Sun & An, 2005) (c) Dust fluxes from ODP 1090 in the South Atlantic (Martínez-Garcia et al., 2011).

accumulation, such as those determined in the CLP (Y. Sun & An, 2005; D. Sun et al., 2008) and South Atlantic (Martínez-Garcia et al., 2011), which display either stable or increasing glacial values when the early and late Pleistocene are considered (Figure 8). Enhanced dust fluxes to the North Pacific Ocean through the Quaternary could be expected due to more expansive Northern Hemisphere ice, lower temperatures, and stronger temperature gradients (Batchelor et al., 2019; Brierley et al., 2009; Herbert et al., 2010; Lisiecki & Raymo, 2005; Roe, 2009; Westerhold et al., 2020). The MARs of loess on the CLP and dust fluxes from the South Atlantic generally follow this conventional expectation, although we do note that (a) neither record uses a CFP for both the early and late Pleistocene and as such are susceptible to distortion associated with changes in sediment redistribution, and (b) the temporal pattern of relative glacial dust fluxes is not entirely consistent between the records across the Quaternary.

While the lack of data from ∼330 to 2,500 ka does not allow us to directly address the evolution of North Pacific dust fluxes through the entire Quaternary, we can still evaluate this incongruity between the global dust flux records, and in turn, address Quaternary landscape evolution in East Asia. Although many possibilities exist, we propose three endmember hypotheses (Figure 9) to explain our findings with the predication that dust production and availability are the predominant drivers of said fluxes. These hypotheses are based on other records of global climate, marine dust fluxes, and East Asian monsoonal variability (Lang et al., 2014; Lisiecki & Raymo, 2005; Martínez-Garcia et al., 2011; Naafs et al., 2012; Wu et al., 2007; Y. G. Zhang et al., 2009), all three of which can be tested by future research.

In Scenario #1, glacial dust fluxes to the North Pacific Ocean decreased steadily through the Pleistocene. One potential mechanism could be related to the progressive erosion of dust-producing surfaces within particular regions, such as the abundant modern stony deserts in the Gobi Desert and within other arid basins across East

10.1029/2022PA004571

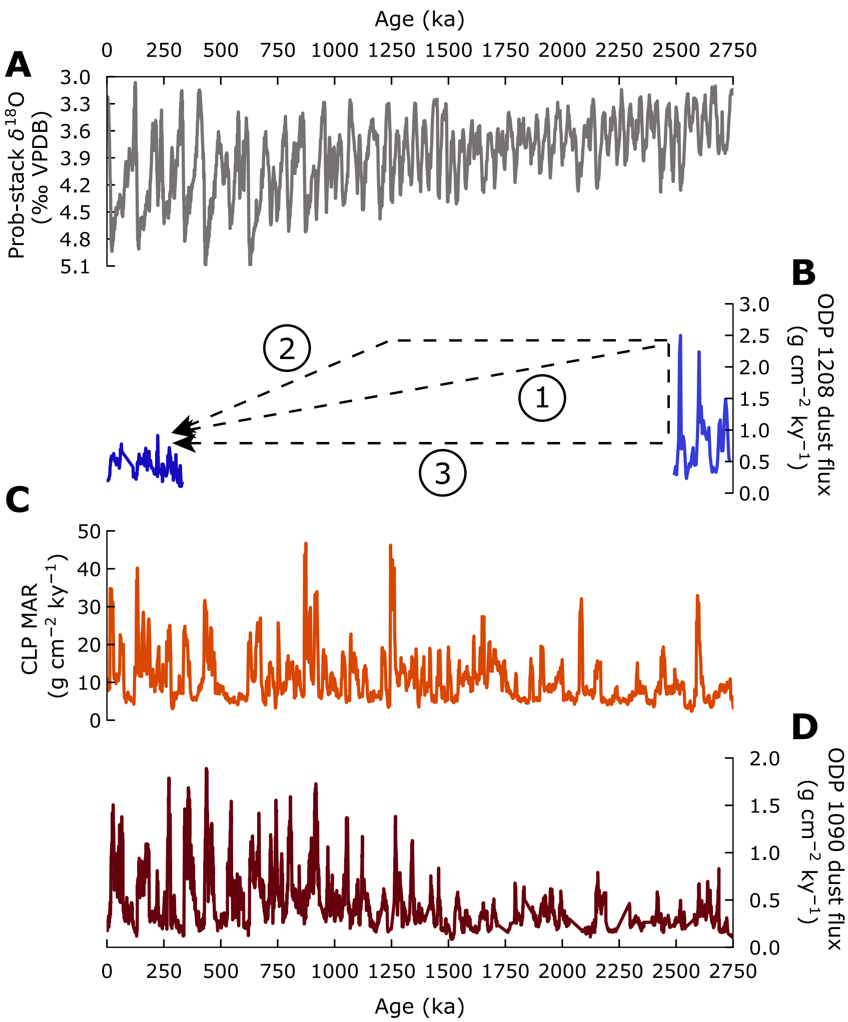

Figure 9. Reconstructions of dust from East Asia, the North Pacific Ocean, and the South Atlantic Ocean. (a) Prob-stack benthic oxygen isotope stack (Ahn et al., 2017). (b) ODP 1208 dust fluxes (based on $^{232}Th_{total}$ concentrations) (Abell et al., 2021; Kinsley, 2019; Kinsley et al., 2022). Error bars removed for clarity. Circled numbers represent possible scenarios for East Asian Pleistocene dust evolution discussed in the text. (1) North Pacific dust fluxes monotonically decrease through the Pleistocene; (2) Dust fluxes remain elevated until the mid-Pleistocene Transition, at which point they decrease steadily to late Pleistocene levels; (3) the first ~250 ky after the intensification of Northern Hemisphere Glaciation are anomalous in terms of dust, and late Pleistocene values are reached immediately after ~2,500 ka. (c) CLP mass accumulation rates (Y. Sun & An, 2005). (d) ODP 1090 dust fluxes (Martínez-Garcia et al., 2011).

Asia (Figure 1) (B. Zhang et al., 2008), becoming depleted in surficial silt- and clay-sized sediment through the Quaternary (Pullen et al., 2018). This is likely not a linear evolution because some climate-driven replenishment of surficial sediment is expected (e.g., Abell et al., 2020b; D. Zhang et al., 2020). The overall effect would be a decreasing sediment supply to dust sources such as the Qaidam Basin, Turpan-Hami Basins, and the spatially expansive Gobi Desert through the Pleistocene. Lacking large glacier systems (outside of high elevation mountain ranges) in the continental interior of East Asia, fluvial erosion of mountain systems bounding these regions is the dominant mechanism of sediment production (Heermance et al., 2013; Jiang & Yang, 2019; Lu et al., 2019b). This evolution contrasts with major dust producing areas such as Patagonia and North America where glaciogenic processes drive Pleistocene sediment supply during glacial intervals (Martínez-Garcia et al., 2011; Naafs et al., 2012). Thus, the observed increase in dust fluxes to the South Atlantic across the Quaternary may be driven by larger late Pleistocene ice sheets in southern South America relative to the early Pleistocene. We also note that the ODP 1208 CFP-derived dust fluxes are above zero, implying a baseline contribution of the continental interior of East Asia. The model of Scenario #1 would ascribe a portion of that baseline to the Tarim Basin and Junggar Basin, which probably followed a much different landscape evolution pathway compared to the stony

10.1029/2022PA004571

desert surfaces. Speculatively, this may be in part because of greater glacio-fluvial sediment production in the western Kunlun and Altai mountains refreshing the Tarim Basin and Junggar Basin, respectively.

The steadily decreasing glacial East Asian dust flux hypothesis requires changes to variables influencing Quaternary local fluvial activity; namely, a decrease in fluvial activity that resulted in lower sediment production and availability, likely during interglacials. Precipitation related to the East Asian summer monsoon was intensified during the Pliocene epoch (Ao et al., 2016; Nie et al., 2014) and potentially decreased through the Pleistocene (Wu et al., 2007; Y. G. Zhang et al., 2009), although this is debated (Meng et al., 2018). Enhanced sediment production via fluvial erosion in warmer climates is supported by modern observations (D. Li et al., 2021). Significant wind erosion of the Qaidam Basin initiated around the Plio-Pleistocene transition, which is also consistent with aridification/lower precipitation at this time (Heermance et al., 2013; Kapp et al., 2011). In terms of landscape evolution, we note an important internal consistency within the framework of this hypothesis: the progressive development of desert pavements in parts of East Asia used as evidence to rationalize this hypothesis has been shown to potentially affect regional atmospheric conditions primarily through altered downwelling radiation and lower regional aerosol concentrations; substantially in some areas (Abell et al., 2020a, 2020b). This surface-atmosphere feedback could have led to suppressed cloud formation and precipitation, and thus forced adjustments to fluvial driven sediment production in regions where landscape evolution occurred. Overall, decreasing regional precipitation, the establishment of the modern Gobi Desert at ~2,600 ka, and its episodic development of stony surfaces (Lu et al., 2019b; Pullen et al., 2018; D. Zhang et al., 2020, 2022), all support elevated late Pliocene–early Pleistocene glacial dust fluxes that transition to lower values by the late Pleistocene.

$^{4}He_{terr}/^{232}Th_{total}$ ratios may also lend support for both short- (glacial-interglacial) and long- (Quaternary) term shifts in dust availability. Utilizing the late Pliocene-early Pleistocene data set, we can rule out a substantial influence by grain size because the ratios display no relationship between the highest values (which would indicate larger grain sizes) and peaks in dust flux (i.e., elevated gustiness/windiness) (Figures S4 and S5 in Supporting Information S1) (Abell et al., 2021; McGee et al., 2010; Rea & Hovan, 1995). However, we find that the ratios of these two dust proxies are weakly related to both volcanic input (Figure S6 in Supporting Information S1) as well as climate (interpreted from benthic $\delta^{18}O$) (Figure 6; Figure S7 in Supporting Information S1). It is reasonable to expect some correlation between volcanics and $^{4}He_{terr}/^{232}Th_{total}$ ratios because of the potentially substantial contribution of volcanically derived ^{232}Th to many of the samples. The equally weak relationship between benthic oxygen isotopes and $^{4}He_{terr}/^{232}Th_{total}$ ratios, on the other hand, potentially offers some insight into an additional mechanism impacting these dust proxies, especially when the lack of correspondence between $^{4}He_{terr}/^{232}Th_{total}$ ratios and overall dust flux is considered. Specifically, we suggest a portion of the variability in the ratio could be related to climatically driven shifts in dust provenance and/or sediment production, based on some variability in $^{4}He_{terr}/^{232}Th$ ratios of East Asian deserts (McGee et al., 2016). On glacial-interglacial timescales, the $^{4}He_{terr}/^{232}Th_{total}$ ratio-climate correspondence may support our argumentation of sediment availability (related to fluvial processes that are ultimately tied to climate) setting the dominant sources of dust, although this could also be driven by the position of the westerlies (see discussion below) (Abell et al., 2021; An et al., 2012). Ultimately, the relationship between climate and $^{4}He_{terr}/^{232}Th$ ratios is weak, and as such our interpretation is speculative. However, regardless of the climate connection, the larger range in $^{4}He_{terr}/^{232}Th$ values found in the late Pliocene-early Pleistocene could reflect the presence of additional sources of dust during the late Pliocene-early Pleistocene—examples would include basins that evolved towards stony surfaces—which would support our explanations based on the dust flux records. One complication under this scenario might be the potential expansion of deserts at ~900–1,100 ka (e.g., Tengger, Hodq, and Badain Jaran) (Z. Li et al., 2014; B. Li et al., 2017; F. Wang et al., 2015; Zhao et al., 2022). Interestingly, this proposed mid-Pleistocene desert expansion is not recorded as a shift in provenance at the CLP during the mid-Pleistocene (e.g., Pullen et al., 2011; J. Zhang et al., 2022). But if valid, it would imply that as some sources made diminishing dust contributions during glacial periods, others may have amplified, but ultimately increasing contributions were outpaced by the diminishing contributors.

Considering these evidences, along with previous interpretations suggesting strengthened westerly winds during glacials after ~2,730 ka (Abell et al., 2021), we propose that during the late Pliocene-early Pleistocene, sediment was readily available to be deflated in numerous arid basins throughout eastern Asia, and large volumes of sediment were exported downwind to the CLP and North Pacific Ocean during glacial intervals. As the Quaternary progressed, generally cooler and more arid conditions decreased sediment production, while wind speeds remained elevated (particularly during colder climates), and as such stony surfaces (e.g., desert pavements) developed and emitted substantial yet proportionately less dust during glacial intervals. Arid regions that were continually replenished with unconsolidated sediments, such as those near the floodplains of major river systems or those bounded by steep topography receiving sufficient precipitation (e.g., the Tarim Basin; Fang et al., 2020), continued to produce considerable quantities of dust in the late Quaternary as other desert regions evolved toward lower dust emissions.

Scenario #2 is similar to the first, except the timing of decreasing glacial dust fluxes is limited to the last ∼750–1,250 ky, coinciding with the mid-Pleistocene Transition (MPT) (Figure 9b). Numerous records mentioned above describe additional changes around this time (Heermance et al., 2013; Wu et al., 2007; Y. G. Zhang et al., 2009), and it is possible that this marked the major transition in East Asian dust fluxes. If we consider strengthened and longer glacial intervals to be representative of weaker East Asian monsoonal systems, and in turn decreased sediment production, then climate transitioning from ∼41 to ∼100-ky cycles at the MPT, along with intensified glacial peaks thereafter (Lisiecki & Raymo, 2005), supports a decrease in dust fluxes to the North Pacific Ocean between the late Pliocene–early Pleistocene and the late Pleistocene-Holocene. The mechanisms would be equivalent to scenario #1, just over a shorter time interval. Interestingly, North Pacific glacial dust fluxes would then be a near "mirror image" of those for the South Atlantic (Figure 9d) (Martínez-Garcia et al., 2011), in that glacial dust fluxes from South America increase across the MPT while those in Eastern Asia decrease. This is consistent with the response of the regional dust production mechanisms to the same forcing (i.e., enhanced glacial periods through the Pleistocene), as larger Patagonian ice fields could enhance sediment production, while lower precipitation and the absence of extensive ice sheets in East Asia would potentially decrease sediment production.

Finally, as indicated by Scenario #3, it is possible that the period around MIS 100–G6 was anomalous in terms of glacial dust fluxes, and as such glacial dust input returned to near late Pleistocene levels soon after ∼2,500 ka (Figure 9). This could occur if much of the sediment produced during the wetter Pliocene (Ao et al., 2016; Nie et al., 2014) was removed via wind during colder periods over the first ∼250 ky after the intensification of Northern Hemisphere Glaciation, and surfaces were not refreshed to the same degree during subsequent wet/dry phases. Interestingly, n-alkane accumulation rates (a proxy for dust) from the North Atlantic presented in Naafs et al. (2012) also show high fluxes during early Pleistocene, although this record is not constrained by CFPs. So, while we posit that this scenario is unlikely, further consideration is warranted given our lack of constraints.

In summary, we propose that changes in precipitation, the intensity and position of near-surface winds, and surficial geology in East Asia could have convolved to produce the decrease in glacial dust fluxes to the North Pacific Ocean from the early to late Quaternary. At minimum, the proposed Earth system feedback processes and our combined dust records raise questions about our current understanding of East Asian dust dynamics over the last ∼2,700 ky, and may aid in distinguishing East Asian dust dynamics from other major dust sources such as North and South America (Martínez-Garcia et al., 2011; Naafs et al., 2012).

We acknowledge that the Quaternary arid-region landscape evolution hypothesis postulated for scenarios #1 and #2 above runs counter to much existing evidence from East Asia, particularly the expansion of loess deposits across East and Central Asia after the Pliocene and through the Quaternary (Lu et al., 2019b; Song et al., 2021; Zeng et al., 2016) and the enhanced accumulation of loess during more arid periods of the mid-to-late Quaternary (G. Li et al., 2020; Y. Sun & An, 2005), which support the classical notion of colder and drier climates driving enhanced dust production and accumulation. Because a nuanced discussion of the details behind each of these hypotheses is not provided here, we do not assert that the latter of the two is incorrect. On the contrary, our aim is to provide an additional, novel hypothesis to consider and test with future work alongside existing interpretations of Quaternary East Asian dust dynamics.

4.3. Variability in the Westerlies and Their Potential Role in Quaternary Glacial Dustiness

Alongside sediment availability, wind is a key driver of dust emission, transport, and deposition (McGee et al., 2010). As such, we must consider variability in the characteristics of relevant wind systems when interpreting the combined Quaternary CFP-derived dust flux record at ODP 1208. Specifically, shifts in the position and intensity of the Northern Hemisphere westerlies over the last ∼2,730 ky could play a substantial role in driving the observed glacial dust flux signal. In fact, changes to this feature of atmospheric circulation has previously been interpreted to influence North Pacific and Sea of Japan dust deposition over a variety of timescales (e.g., Abell et al., 2021; Lee et al., 2022; Nagashima et al., 2011; Tang et al., 2022).

If one were to use the conclusions of Abell et al. (2021), who state that the westerlies move equatorward and intensify during glacials after the intensification of Northern Hemisphere Glaciation due to the development of ice sheets and strengthened meridional temperature gradients, then it may be suggested that during progressively more intense glacials such as those found during the late Quaternary, the westerlies could hypothetically shift so far south that ODP 1208 would have received less Asian dust during glacials at some point in the Quaternary. In fact, recent work has put forth this exact mechanism to explain decreased n-alkane fluxes to the mid-latitude North Pacific after the Mid-Bruhnes Event (Jonas et al., 2023). We can evaluate this hypothesis considering our three proposed scenarios described above along with the major assumption that, outside of climatic thresholds, the position and intensity of the westerlies scale with meridional temperature gradients and ice volume. Scenario #3 cannot be invoked if the westerlies are responsible for driving the decreasing glacial dust fluxes at ODP 1208, as there is no apparent climatic reason (at least related to ice volume and meridional temperature gradients) why the westerlies would change dramatically after ~2,500 ka. As for scenarios #1 and #2, we postulate that it would likely be some combination of the two that would be needed to reasonably explain our dust fluxes at ODP 1208. Specifically, there could be a roughly monotonic decline in glacial dust fluxes that scales with glacial benthic oxygen isotopes from ~2,700 ka to ~600–700 ka (Figure 9). Following this interval, when glacial benthic oxygen isotopes reach their maximum glacial values for the Quaternary, the westerlies would have reached their maximum glacial equatorward position, and in turn glacial dust fluxes to the mid-latitude North Pacific would remain relatively constant (assuming no major change in East Asian desert surficial conditions). We note that average late Pleistocene glacial dust fluxes at ODP 1208 are similar in magnitude, which may support the proposed westerly wind-driven dust flux evolution (Figure 5 and Table 1). Future work generating CFP-derived dust fluxes from marine sediments located in the mid-latitude North Pacific spanning the period of ~0–1,000 ka would be valuable for assessing the feasibility of this hypothesis.

While the shifting westerlies hypothesis is plausible, there are several caveats that must be discussed. ODP 1208 lies within a few degrees of latitude of the main axis of the westerly winds over the North Pacific today. Considering modeling output of dust deposition to the Pacific Ocean (e.g., Albani et al., 2014), it would likely require an extreme shift of the westerlies between late Pliocene-early Pleistocene glacials and those of the late Pleistocene in order to produce the approximately two-fold reduction in glacial dust deposition observed at ODP 1208. Jonas et al. (2023) suggest that this major positional change in the westerlies could occur if the westerly jet stream was permanently located south of the Tibetan Plateau during peak glacial conditions. At present, the results from other proxy and modeling work could be used to both confirm or reject this notion (e.g., Gray et al., 2020; Lei et al., 2021; N. Wang et al., 2018). We note that the hypothesis of Jonas et al. (2023) could explain the relatively similar glacial dust fluxes at ODP 1208 during the late Pleistocene, as the westerlies would be located south of major dust sources during each one of these glacial intervals. However, this leaves the question of why, if the westerlies are no longer located over major Asian dust source regions, dust is still higher during glacials compared to interglacials in the mid-latitude and subarctic North Pacific, which has been widely observed (Hovan et al., 1991; Kawahata et al., 2000; Maeda et al., 2002; Rea & Leinen, 1988; Serno et al., 2017; Xu et al., 2015). Ultimately, further work is needed to evaluate the validity of this interpretation.

We note that if changes in atmospheric circulation are the dominant mechanism behind the decreasing mid-latitude glacial dust fluxes presented here, then our use of singular records from either terrestrial or marine archives to infer temporal variability in dust dynamics is potentially problematic. In other words, if shifts in the position and intensity of winds, as well as dust production mechanisms, are all influencing the final dust deposition signal, then analysis of multiple, spatially distinct dust flux records based on a high-resolution, multi-proxy approach may be necessary to produce meaningful interpretations about each of these components of the climate system.

4.4. $^3He_{ET}$ in the Late Pliocene—Early Pleistocene: A Problem of "Constant"?

Our ability to constrain the absolute values of late Pliocene-early Pleistocene dust fluxes to ODP 1208 is sensitive to the choice of the value of the flux of $^3He_{ET}$ to Earth (F_{3HeET}), and thus our conclusions could be biased if F_{3HeET} was different in the past. For completeness, here we address the question of the value of the flux of $^3He_{ET}$ to Earth in the late Pliocene–early Pleistocene.

To our knowledge, there are only two studies that provide estimates for Pliocene and early Pleistocene F_{3HeET} (Farley, 1995; Graham & Konrad, 2022). Farley (1995) determined that F_{3HeET} for the Pliocene ranged from ~0.2 to 0.65 pcc cm^{-2} ky^{-1} (Pliocene Epoch average: ~0.6 pcc cm^{-2} ky^{-1}), while Graham and Konrad (2022) suggested a median F_{3HeET} of 0.88 ± 0.26 pcc cm^{-2} ky^{-1} over the interval of ~1,700–3,200 ka. However, these values are based on traditional age model-derived MARs (Farley, 1995; Graham & Konrad, 2022), and thus may be biased by local sedimentary environments. Because the potential influence of sediment redistribution on flux estimates is one of the reasons CFPs are widely utilized, this method of constraining F_{3HeET} is problematic and carries nontrivial uncertainty. Nonetheless, the application of $^{3}He_{ET}$ for this interval is necessary because it is the only CFP suitable for work encompassing sediments older than ~500 ky, as the half-life of ^{230}Th (~75 ky) precludes its use beyond this point (Costa et al., 2020; McGee & Mukhopadhyay, 2013).

In light of these considerations, we use $^{3}He_{ET}$-derived dust fluxes based on the assumption that the Quaternary F_{3HeET} of 0.8 ± 0.3 [1σ] pcc cm^{-2} ky^{-1} (McGee & Mukhopadhyay, 2013) holds for the last ~2,730 ky, following Abell et al. (2021). This approach is likely as uncertain as the Pliocene values determined via traditional age model-derived MARs. However, we stress that the number selected for F_{3HeET} only impacts the absolute values of the dust fluxes, and not the variability between samples. In Text S3 of the Supporting Information S1, we describe that by utilizing a reasonably lower F_{3HeET} value, late Pliocene-early Pleistocene glacial dust fluxes are still greater than the late Pleistocene, and as such the enhanced glacial-interglacial variability in the earlier interval remains as well. With this in mind, we suggest that until future work is able to better constrain F_{3HeET} for time intervals prior to the late Quaternary, our combined dust flux record for ODP 1208 remains valid, as do the associated interpretations.

4.5. Potential Implications for the Chinese Loess Plateau

The dissimilarities between the late Pliocene–early Pleistocene and late Pleistocene glacial dust fluxes to the mid-latitude North Pacific and the CLP warrants consideration (Figures 8 and 9). The glacial MARs at the CLP do not show a decrease across the Pleistocene like the ODP 1208 record, but rather increase (on average) throughout the Pleistocene (Figure 9c). The CLP record also largely shows higher amplitude changes in MARs starting around the beginning of the MPT (~1,250 ka) and continuing to the Holocene, unlike ODP 1208 where large amplitude changes are observable in the late Pliocene-early Pleistocene and likely decrease along with the proposed decreasing glacial average dust flux. These observations imply glacial dust fluxes to the CLP and mid-latitude North Pacific resulted from different processes and dynamics, and that one record is not always a reasonable substitute for the other.

Aside from the caveats mentioned for dust flux reconstructions at ODP 1208 earlier in the Discussion, the disparate Pleistocene dust flux histories for ODP 1208 and CLP could potentially be explained by (a) spatially distinct local sources of CLP sediments (Nie et al., 2015; H. Zhang et al., 2021), (b) the different dominant atmospheric circulation patterns driving CLP and ODP 1208 dust delivery (i.e., westerlies vs. the EAWM; see Discussion Section 4.3 above) (Gao et al., 2021), and (c) expansion of the bedrock-floored Mu Us desert—through eolian deflation—coupled with retreat of the windward margin of the CLP through wind erosion (e.g., Ding et al., 2005; Kapp et al., 2015; Qiang et al., 2021; Xu et al., 2018).

For point #1, we note most of the stony desert surfaces we invoke for our posited dust production-related driver of decreasing glacial dust delivered to the North Pacific are located latitudinally north of the CLP, and within the path of the modern-day westerlies. This may imply the suppression of dust emission from development of these stony surfaces was less impactful on the rate of dust accumulation at the CLP than for the mid-latitude North Pacific Ocean. More broadly, it is probable that North Pacific dust integrates windblown sediment from a much larger range of sources than the CLP, including but not limited to, the Tarim Basin, Junggar Basin, Qaidam Basin, Hexi Corridor, Tengger Desert, Badain Jaran Desert, Mu Us Desert, and Gobi Desert (Shao & Dong, 2006; X.-Y. Zhang et al., 2003; Q. Zhang et al., 2020b). Because of their location, many of these sources likely play a much less substantial role for the CLP, a premise that is also supported by the current understanding of the provenance of Quaternary CLP strata, which are thought to be primarily sourced from the Yellow River (floodplain) and Mu Us Desert (Nie et al., 2015; H. Zhang et al., 2021).

In regards to point #3, several pieces of evidence, including (a) wind eroded linear loess topography, (b) the deeply incised high topographical escarpment on the windward side of the CLP adjacent to the Mu Us, (c) thinning Pleistocene loess-paleosol stratigraphy across the CLP in the downwind direction, and (d) the presence of ~10^4 yr-long unconformities in the late Pleistocene CLP stratigraphy along the topographical escarpment, all support the hypothesis that the CLP was extensively eroded by the wind during at least the late Pleistocene (Ding et al., 2005; Kapp et al., 2015; Stevens et al., 2018). A wind eroded CLP margin adjacent to the Mu Us implies deflation and transport of dust over the interior of the CLP by the prevailing westerly–northwesterly winds. Interestingly, while Stevens et al. (2018) show ∼10^4 yr-long unconformities on the ablative margin of the CLP, a record by J. Zhang et al. (2022) indicates continuous dust accumulation within the central CLP. Thus, in this model, as the Mu Us margin of the CLP was eroded, the dust was carried to the interior of the CLP, and a portion out to the North Pacific Ocean. Based on Ding et al. (2005) we speculate that this process may have started by the MPT (∼1,200 ka) or during the intensification of Northern Hemisphere Glaciation (∼2,730 ka). If this hypothesis is valid, it entails the CLP being both a depositional center and point source for Pleistocene dust. Additionally, the hypothesis implies that at least some CLP MAR records are incomplete and inaccurate proxies for East Asian dust production during the Pleistocene, but could perhaps more accurate proxies for deflation of the Mu Us, erosion and internal recycling of the CLP, or of localized detrital input.

We again note that evidence exists which could be used to refute our explanation for the discrepancies between our marine-based dust flux record and those from the CLP. With this in mind, we do not suggest our interpretations provide an all-encompassing solution to this conundrum, but instead stress the importance of accurate contextualization of proxies such as loess MARs and grain size from the CLP and dust fluxes from the mid-latitude North Pacific Ocean.

5. Perspective and Conclusions

The combined CFP-derived dust flux reconstructions and dust proxy data from ODP 1208 presented here provides a new perspective on the evolution of East Asian dust dynamics since the intensification of Northern Hemisphere Glaciation at ∼2,730 ka. Our findings are consistent with a dust production framework that incorporates landscape and climate evolution across the Quaternary, although the detailed timing of its evolution is yet to be constrained. If valid, the interpretation of decreased glacial dust across the past ∼2,730 ky highlights the importance of considering region-specific mechanisms associated with sediment availability, ice dynamics, precipitation, and the variability of surficial geology in dust-producing areas. However, we note that much more work is necessary to evaluate this proposed hypothesis in the context of contrasting data and interpretations on East Asian dust dynamics.

If dust production is not the dominant mechanism behind our record, we also highlight the potential for atmospheric circulation to be an important driver of our observed decreasing glacial dust fluxes, but note some caveats that need to be further explored to validate our interpretation. Regardless, if correct, this westerly wind hypothesis would further emphasize the need to consider dust flux data from a much wider spatial extent to better constrain potential interpretations of Asian dust dynamics (i.e., a single record is useful, but may allow for multiple interpretations—this study is one such example).

We also find that our ODP 1208 record is at odds with previous work from the North Pacific Ocean, Sea of Japan, and CLP. Importantly, these latter records are somewhat inconsistent with one another even if our new dust reconstruction is ignored. Using our new data, we attribute these discrepancies to uncertainties inherent to the flux determinations from previous studies that may prove problematic for these records as reliable archives. We do not describe the uncertainties related to each of these dust records to explicitly preclude their use in examining East Asian dust dynamics, but do so to emphasize the differences between them and provide the reader with a sense of the available data from which we draw our current understanding of the mechanisms driving changes in Quaternary dust originating from the deserts and arid regions of East Asia. Considering the substantial differences, we stress the need for records of dust flux from archives downwind of East Asia that satisfy the following conditions: (a) include high-resolution sampling; (b) are constrained by reliable age models; (c) have minimal inputs of non-dust lithogenic sources such as ice-rafted debris and riverine sediments; (d) can be corrected for volcanic contributions by geochemical methods such as the use of multiple elemental and isotopic proxies or multivariate statistical endmember modeling; (e) apply CFPs to accurately determine fluxes; and (f) do not include localized recycling of sediment which possibly obscures the regional dust signal, as is potentially the case for the CLP. Having such records will be essential for providing insight into research on: (a) the dominant modes of sediment production, transport, and deposition since the inception of major Northern Hemisphere ice sheets; (b) the presence of active sources in the early to mid-Pleistocene that were no longer producing dust in the late Pleistocene but may become relevant under changing climate conditions; (c) how and when bedrock-floored and desert pavement-mantled surfaces originated in East Asia; (d) how atmospheric circulation may have shifted during glacial periods across the Quaternary; and finally, (e) the potential for a decoupled CLP and North Pacific Ocean in terms of what these dust archives can reveal about regional climate.

Conflict of Interest

The authors declare no conflicts of interest relevant to this study.

Data Availability Statement

Original dust data is from Abell et al. (2021), Kinsley (2019), Kinsley et al. (2022), and McGee et al. (2016). All new data and results can be found in data set file Data Set S1 (Abell, 2023b) stored in the figshare.com data repository. The code files for the analyses performed on the dust data (Abell, 2023a) can be found in the figshare.com data repository.

Acknowledgments

We thank Chloe Anderson and Joshua Bridges for helpful discussions that improved this manuscript. All ODP 1208 core samples were originally provided by the International Ocean Discovery Program (IODP). IODP is sponsored by the U.S. National Science Foundation (NSF) and participating countries under the management of Joint Oceanographic Institutions, Inc. This research was funded in part by the U.S. National Science Foundation (NSF-PIRE 1545859 to G. W., A. P., and P. A. K.; NSF-OCE 1436014 to H.L.F. and M.E.R). J. T. A. was supported during his graduate work by the U.S. National Science Foundation (NSF-PIRE 1545859) and is currently supported by the U.S. National Science Foundation (NSF-OCE-PRF 2126500).

References

Abell, J. T. (2023a). Abell et al. Python code files [Software]. Figshare. https://doi.org/10.6084/m9.figshare.21375852

Abell, J. T. (2023b). Abell et al. supplementary dataset S1 [Dataset]. Figshare. https://doi.org/10.6084/m9.figshare.20219985

Abell, J. T., Pullen, A., Lebo, Z. J., Kapp, P., Gloege, L., Metcalf, A. R., et al. (2020a). A wind-albedo-wind feedback driven by landscape evolution. *Nature Communications*, *11*(1), 1–9. https://doi.org/10.1038/s41467-019-13661-w

Abell, J. T., Rahimi, S. R., Pullen, A., Lebo, Z. J., Zhang, D., Kapp, P., et al. (2020b). A quantitative model-based assessment of stony desert landscape evolution in the Hami Basin, China: Implications for Plio-Pleistocene dust production in eastern Asia. *Geophysical Research Letters*, *47*(20), e2020GL090064. https://doi.org/10.1029/2020GL090064

Abell, J. T., Winckler, G., Anderson, R. F., & Herbert, T. D. (2021). Poleward and weakened westerlies during Pliocene warmth. *Nature*, *589*(7840), 70–75. https://doi.org/10.1038/s41586-020-03062-1

Ahn, S., Khider, D., Lisiecki, L. E., & Lawrence, C. E. (2017). A probabilistic Pliocene–Pleistocene stack of benthic $\delta^{18}O$ using a profile hidden Markov model. *Dynamics and Statistics of the Climate System*, *2*(1). https://doi.org/10.1093/climsys/dzx002

Albani, S., Mahowald, N., Perry, A., Scanza, R., Zender, C., Heavens, N., et al. (2014). Improved dust representation in the Community Atmosphere Model. *Journal of Advances in Modeling Earth Systems*, *6*(3), 541–570. https://doi.org/10.1002/2013ms000279

An, Z., Colman, S. M., Zhou, W., Li, X., Brown, E. T., Jull, A. T., et al. (2012). Interplay between the Westerlies and Asian monsoon recorded in Lake Qinghai sediments since 32 ka. *Scientific Reports*, *2*(1), 619. https://doi.org/10.1038/srep00619

Anderson, C. H., Murray, R. W., Dunlea, A. G., Giosan, L., Kinsley, C. W., McGee, D., & Tada, R. (2020). Aeolian delivery to Ulleung Basin, Korea (Japan Sea), during development of the East Asian Monsoon through the last 12 Ma. *Geological Magazine*, *157*(5), 806–817. https://doi.org/10.1017/s001675681900013x

Ao, H., Roberts, A. P., Dekkers, M. J., Liu, X., Rohling, E. J., Shi, Z., et al. (2016). Late Miocene–Pliocene Asian monsoon intensification linked to Antarctic ice-sheet growth. *Earth and Planetary Science Letters*, *444*, 75–87. https://doi.org/10.1016/j.epsl.2016.03.028

Bailey, I., Liu, Q., Swann, G. E., Jiang, Z., Sun, Y., Zhao, X., & Roberts, A. P. (2011). Iron fertilization and biogeochemical cycles in the sub-Arctic northwest Pacific during the late Pliocene intensification of northern hemisphere glaciation. *Earth and Planetary Science Letters*, *307*(3–4), 253–265. https://doi.org/10.1016/j.epsl.2011.05.029

Batchelor, C. L., Margold, M., Krapp, M., Murton, D. K., Dalton, A. S., Gibbard, P. L., et al. (2019). The configuration of Northern Hemisphere ice sheets through the Quaternary. *Nature Communications*, *10*(1), 1–10. https://doi.org/10.1038/s41467-019-11601-2

Bralower, T., Premoli Silva, I., & Malone, M. (2002). Leg 198. *Proceedings of the Ocean Drilling Program: Initial Reports*, *198*, 148.

Bridges, J., Tarduno, J., & Cottrell, R. (2021). A critical review of North Pacific red clay sediments and their paleoclimatic significance. In *Presented at the 2021 American geophyscial union fall meeting* (Vol. PP53A-04). AGU.

Brierley, C. M., Fedorov, A. V., Liu, Z., Herbert, T. D., Lawrence, K. T., & LaRiviere, J. P. (2009). Greatly expanded tropical warm pool and weakened Hadley circulation in the early Pliocene. *Science*, *323*(5922), 1714–1718. https://doi.org/10.1126/science.1167625

Butcher, S., King, T., & Zalewski, L. (2017). *Apocrita-high performance computing cluster for queen*. Mary University of London.

Costa, K. M., Hayes, C. T., Anderson, R. F., Pavia, F. J., Bausch, A., Deng, F., et al. (2020). ^{230}Th normalization: New insights on an essential tool for quantifying sedimentary fluxes in the modern and Quaternary Ocean. *Paleoceanography and Paleoclimatology*, *35*(2), e2019PA003820. https://doi.org/10.1029/2019pa003820

Ding, Z., Derbyshire, E., Yang, S., Sun, J., & Liu, T. (2005). Stepwise expansion of desert environment across northern China in the past 3.5 Ma and implications for monsoon evolution. *Earth and Planetary Science Letters*, *237*(1–2), 45–55. https://doi.org/10.1016/j.epsl.2005.06.036

Dunlea, A. G., Murray, R. W., Sauvage, J., Spivack, A. J., Harris, R. N., & D'Hondt, S. (2015). Dust, volcanic ash, and the evolution of the South Pacific Gyre through the Cenozoic. *Paleoceanography*, *30*(8), 1078–1099. https://doi.org/10.1002/2015pa002829

Fang, X., An, Z., Clemens, S. C., Zan, J., Shi, Z., Yang, S., & Han, W. (2020). The 3.6-Ma aridity and westerlies history over midlatitude Asia linked with global climatic cooling. *Proceedings of the National Academy of Sciences of the United States of America*, *117*(40), 24729–24734. https://doi.org/10.1073/pnas.1922710117

Farley, K. A. (1995). Cenozoic variations in the flux of interplanetary dust recorded by ^{3}He in a deep-sea sediment. *Nature*, *376*(6536), 153–156. https://doi.org/10.1038/376153a0

Farley, K. A., Love, S., & Patterson, D. B. (1997). Atmospheric entry heating and helium retentivity of interplanetary dust particles. *Geochimica et Cosmochimica Acta*, *61*(11), 2309–2316. https://doi.org/10.1016/s0016-7037(97)00068-9

Ford, H. L., & Raymo, M. E. (2020). Regional and global signals in seawater $\delta^{18}O$ records across the mid-Pleistocene transition. *Geology*, *48*(2), 113–117. https://doi.org/10.1130/g46546.1

Gallagher, S. J., Kitamura, A., Iryu, Y., Itaki, T., Koizumi, I., & Hoiles, P. W. (2015). The Pliocene to recent history of the Kuroshio and Tsushima Currents: A multi-proxy approach. *Progress in Earth and Planetary Science*, *2*(1), 17. https://doi.org/10.1186/s40645-015-0045-6

Gao, X., Hao, Q., Ge, J., Han, L., Fu, Y., Wu, X., et al. (2021). Paleowind directions from the magnetic fabric of loess deposits in the western Chinese Loess Plateau and implications for dust provenance. *Quaternary Research*, *103*, 1–14. https://doi.org/10.1017/qua.2021.5

Graham, D. W., & Konrad, K. (2022). Supernova versus cosmic ray origin for exotic nuclides in geomaterials: A test using ^{3}He with ^{60}Fe in marine sediments. *Geochimica et Cosmochimica Acta*, *336*, 177–187. https://doi.org/10.1016/j.gca.2022.09.016

Gray, W. R., Wills, R. C., Rae, J. W., Burke, A., Ivanovic, R. F., Roberts, W. H., et al. (2020). Wind-driven evolution of the North Pacific subpolar gyre over the last deglaciation. *Geophysical Research Letters*, *47*(6), e2019GL086328. https://doi.org/10.1029/2019gl086328

Gylesjö, S. (2005). 19. Data report: Late Pleistocene terrigenous input to Shatsky Rise, Site 1208.

Hase, H., Yoon, J.-H., & Koterayama, W. (1999). The current structure of the Tsushima Warm Current along the Japanese coast. *Journal of Oceanography*, *55*(2), 217–235. https://doi.org/10.1023/a:1007894030095

Haug, G. H., Maslin, M., Sarnthein, M., Stax, R., & Tiedemann, R. (1995). Evolution of northwest Pacific sedimentation patterns since 6 Ma (Site 882). *Proceedings of the Ocean Drilling Program: Scientific Results*, *293*.

Haug, G. H., Sigman, D. M., Tiedemann, R., Pedersen, T. F., & Sarnthein, M. (1999). Onset of permanent stratification in the subarctic Pacific Ocean. *Nature*, *401*(6755), 779–782. https://doi.org/10.1038/44550

Heermance, R. V., Pullen, A., Kapp, P., Garzione, C. N., Bogue, S., Ding, L., & Song, P. (2013). Climatic and tectonic controls on sedimentation and erosion during the Pliocene–Quaternary in the Qaidam Basin (China). *Bulletin*, *125*(5–6), 833–856. https://doi.org/10.1130/b30748.1

Herbert, T. D., Peterson, L. C., Lawrence, K. T., & Liu, Z. (2010). Tropical ocean temperatures over the past 3.5 million years. *Science*, *328*(5985), 1530–1534. https://doi.org/10.1126/science.1185435

Hovan, S. A., Rea, D. K., & Pisias, N. G. (1991). Late Pleistocene continental climate and oceanic variability recorded in northwest Pacific sediments. *Paleoceanography*, *6*(3), 349–370. https://doi.org/10.1029/91pa00559

Janecek, T. R., & Rea, D. K. (1983). Eolian deposition in the northeast Pacific Ocean: Cenozoic history of atmospheric circulation. *Geological Society of America Bulletin*, *94*(6), 730–738. https://doi.org/10.1130/0016-7606(1983)94<730:editnp>2.0.co;2

Jiang, Q., & Yang, X. (2019). Sedimentological and geochemical composition of aeolian sediments in the Taklamakan desert: Implications for provenance and sediment supply mechanisms. *Journal of Geophysical Research: Earth Surface*, *124*(5), 1217–1237. https://doi.org/10.1029/2018jf004990

Jonas, A.-S., Kars, M., Bauersachs, T., Ruebsam, W., & Schwark, L. (2023). Southward displacement of the glacial westerly jet over Asia driven by enhanced Arctic amplification after the Mid-Brunhes Event. *Global and Planetary Change*, *227*, 104173. https://doi.org/10.1016/j.gloplacha.2023.104173

Kapp, P., Pelletier, J. D., Rohrmann, A., Heermance, R., Russell, J., & Ding, L. (2011). Wind erosion in the Qaidam basin, central Asia: Implications for tectonics, paleoclimate, and the source of the Loess Plateau. *Geological Society of America Today*, *21*(4/5), 4–10. https://doi.org/10.1130/gsatg99a.1

Kapp, P., Pullen, A., Pelletier, J. D., Russell, J., Goodman, P., & Cai, F. (2015). From dust to dust: Quaternary wind erosion of the Mu Us Desert and Loess Plateau, China. *Geology*, *43*(9), 835–838. https://doi.org/10.1130/g36724.1

Kawahata, H., Okamoto, T., Matsumoto, E., & Ujiie, H. (2000). Fluctuations of eolian flux and ocean productivity in the mid-latitude North Pacific during the last 200 Kyr. *Quaternary Science Reviews*, *19*(13), 1279–1291. https://doi.org/10.1016/s0277-3791(99)00096-7

Kienast, S. S., Winckler, G., Lippold, J., Albani, S., & Mahowald, N. M. (2016). Tracing dust input to the global ocean using thorium isotopes in marine sediments: ThoroMap. *Global Biogeochemical Cycles*, *30*(10), 1526–1541. https://doi.org/10.1002/2016gb005408

Kim, K., Chang, K.-I., Kang, D.-J., Kim, Y. H., & Lee, J.-H. (2008). Review of recent findings on the water masses and circulation in the East Sea (Sea of Japan). *Journal of Oceanography*, *64*(5), 721–735. https://doi.org/10.1007/s10872-008-0061-x

Kinsley, C. W. (2019). Reconstructing atmospheric changes in monsoon regions using eolian dust. (Ph.D.). Massachusetts Institute of Technology. Retrieved from https://hdl.handle.net/1721.1/123739

Kinsley, C. W., Bradtmiller, L. I., Zhang, Y., Perala-Dewey, J., & McGee, D. (2022). Ocean-atmosphere changes in the midlatitude North Pacific over the last 330 ka: Dust, biogenic sediment and authigenic uranium accumulation at Shatsky Rise. (Version 1) [Dataset]. Zenodo. https://doi.org/10.5281/zenodo.6791725

Kok, J. F., Adebiyi, A. A., Albani, S., Balkanski, Y., Checa-Garcia, R., Chin, M., et al. (2021). Contribution of the world's main dust source regions to the global cycle of desert dust. *Atmospheric Chemistry and Physics Discussions*, *21*(10), 1–34. https://doi.org/10.5194/acp-21-8169-2021

Lang, D. C., Bailey, I., Wilson, P. A., Beer, C. J., Bolton, C. T., Friedrich, O., et al. (2014). The transition on North America from the warm humid Pliocene to the glaciated Quaternary traced by eolian dust deposition at a benchmark North Atlantic Ocean drill site. *Quaternary Science Reviews*, *93*, 125–141. https://doi.org/10.1016/j.quascirev.2014.04.005

Laurent, B., Marticorena, B., Bergametti, G., Chazette, P., Maignan, F., & Schmechtig, C. (2005). Simulation of the mineral dust emission frequencies from desert areas of China and Mongolia using an aerodynamic roughness length map derived from the POLDER/ADEOS 1 surface products. *Journal of Geophysical Research*, *110*(D18), D18S04. https://doi.org/10.1029/2004jd005013

Lee, A. M., Maruyama, A., Lu, S., Yamashita, Y., Irino, T., & Billi, A. (2022). Quantification of Asian dust source variabilities in silt and clay fractions since 10 Ma by parallel factor (PARAFAC) endmember modeling at IODP Site U1425 in the Japan Sea. *Lithosphere*, *2022*(Special 9). https://doi.org/10.2113/2022/6818103

Lei, J., Shi, Z., Xie, X., Sha, Y., Li, X., Liu, X., & An, Z. (2021). Seasonal variation of the westerly jet over Asia in the Last Glacial Maximum: Role of the Tibetan Plateau heating. *Journal of Climate*, *34*(7), 2723–2740. https://doi.org/10.1175/jcli-d-20-0438.1

Li, B., Sun, D., Xu, W., Wang, F., Liang, B., Ma, Z., et al. (2017). Paleomagnetic chronology and paleoenvironmental records from drill cores from the Hetao Basin and their implications for the formation of the Hobq Desert and the Yellow River. *Quaternary Science Reviews*, *156*, 69–89. https://doi.org/10.1016/j.quascirev.2016.11.023

Li, D., Lu, X., Overeem, I., Walling, D. E., Syvitski, J., Kettner, A. J., et al. (2021). Exceptional increases in fluvial sediment fluxes in a warmer and wetter High Mountain Asia. *Science*, *374*(6567), 599–603. https://doi.org/10.1126/science.abi9649

Li, G., Yang, H., Stevens, T., Zhang, X., Zhang, H., Wei, H., et al. (2020). Differential ice volume and orbital modulation of Quaternary moisture patterns between Central and East Asia. *Earth and Planetary Science Letters*, *530*, 115901. https://doi.org/10.1016/j.epsl.2019.115901

Li, Z., Sun, D., Chen, F., Wang, F., Zhang, Y., Guo, F., et al. (2014). Chronology and paleoenvironmental records of a drill core in the central Tengger Desert of China. *Quaternary Science Reviews*, *85*, 85–98. https://doi.org/10.1016/j.quascirev.2013.12.003

Licht, A., Pullen, A., Kapp, P., Abell, J., & Giesler, N. (2016). Eolian cannibalism: Reworked loess and fluvial sediment as the main sources of the Chinese Loess Plateau. *Bulletin*, *128*(5–6), 944–956. https://doi.org/10.1130/b31375.1

Lin, L., Khider, D., Lisiecki, L. E., & Lawrence, C. E. (2014). Probabilistic sequence alignment of stratigraphic records. *Paleoceanography*, *29*(10), 976–989. https://doi.org/10.1002/2014pa002713

Lisiecki, L. E., & Raymo, M. E. (2005). A Pliocene-Pleistocene stack of 57 globally distributed benthic δ^{18}O records. *Paleoceanography*, *20*(1), PA1003. https://doi.org/10.1029/2004pa001071

Lu, H., Liu, W., Yang, H., Wang, H., Liu, Z., Leng, Q., et al. (2019a). 800-Kyr land temperature variations modulated by vegetation changes on Chinese Loess Plateau. *Nature Communications*, *10*(1), 1–10. https://doi.org/10.1038/s41467-019-09978-1

Lu, H., Wang, X., Wang, X., Chang, X., Zhang, H., Xu, Z., et al. (2019b). Formation and evolution of Gobi Desert in central and eastern Asia. *Earth-Science Reviews*, *194*, 251–263. https://doi.org/10.1016/j.earscirev.2019.04.014

Maeda, L., Kawahata, H., & Nohara, M. (2002). Fluctuation of biogenic and abiogenic sedimentation on the Shatsky Rise in the western North Pacific during the late Quaternary. *Marine Geology*, *189*(3–4), 197–214. https://doi.org/10.1016/s0025-3227(02)00405-x

Marcantonio, F., Kumar, N., Stute, M., Anderson, R. F., Seidl, M. A., Schlosser, P., & Mix, A. (1995). A comparative study of accumulation rates derived by He and Th isotope analysis of marine sediments. *Earth and Planetary Science Letters*, *133*(3–4), 549–555. https://doi.org/10.1016/0012-821x(95)00079-r

Martínez-Garcia, A., Rosell-Melé, A., Jaccard, S. L., Geibert, W., Sigman, D. M., & Haug, G. H. (2011). Southern Ocean dust–climate coupling over the past four million years. *Nature*, *476*(7360), 312–315. https://doi.org/10.1038/nature10310

Masuda, Y., & Aoki, K.-I. (1979). Trace element variations in the volcanic rocks from the Nasu zone, northeast Japan. *Earth and Planetary Science Letters*, *44*(1), 139–149. https://doi.org/10.1016/0012-821x(79)90014-1

McCarron, A., Bigg, G., Brooks, H., Leng, M., Marshall, J., Ponomareva, V., et al. (2020). Northwest Pacific ice-rafted debris at 38°N reveals episodic ice-sheet change in late Quaternary Northeast Siberia. *Earth and Planetary Science Letters*, *553*, 116650. https://doi.org/10.1016/j.epsl.2020.116650

McGee, D., Broecker, W. S., & Winckler, G. (2010). Gustiness: The driver of glacial dustiness? *Quaternary Science Reviews*, *29*(17–18), 2340–2350. https://doi.org/10.1016/j.quascirev.2010.06.009

McGee, D., & Mukhopadhyay, S. (2013). Extraterrestrial He in sediments: From recorder of asteroid collisions to timekeeper of global environmental changes. In *The noble gases as geochemical tracers* (pp. 155–176). Springer.

McGee, D., Winckler, G., Borunda, A., Serno, S., Anderson, R. F., Recasens, C., et al. (2016). Tracking eolian dust with helium and thorium: Impacts of grain size and provenance. *Geochimica et Cosmochimica Acta*, *175*, 47–67. https://doi.org/10.1016/j.gca.2015.11.023

Meng, X., Liu, L., Wang, X. T., Balsam, W., Chen, J., & Ji, J. (2018). Mineralogical evidence of reduced East Asian summer monsoon rainfall on the Chinese Loess plateau during the early Pleistocene interglacials. *Earth and Planetary Science Letters*, *486*, 61–69. https://doi.org/10.1016/j.epsl.2017.12.048

Middleton, J. L., Langmuir, C. H., Mukhopadhyay, S., McManus, J. F., & Mitrovica, J. X. (2016). Hydrothermal iron flux variability following rapid sea level changes. *Geophysical Research Letters*, *43*(8), 3848–3856. https://doi.org/10.1002/2016gl068408

Middleton, J. L., Mukhopadhyay, S., Langmuir, C. H., McManus, J. F., & Huybers, P. J. (2018). Millennial-scale variations in dustiness recorded in Mid-Atlantic sediments from 0 to 70 ka. *Earth and Planetary Science Letters*, *482*, 12–22. https://doi.org/10.1016/j.epsl.2017.10.034

Miller, R. L., Knippertz, P., García-Pando, C. P., Perlwitz, J. P., & Tegen, I. (2014). Impact of dust radiative forcing upon climate. In *Mineral dust* (pp. 327–357). Springer.

Naafs, B. D. A., Hefter, J., Acton, G., Haug, G. H., Martínez-Garcia, A., Pancost, R., & Stein, R. (2012). Strengthening of North American dust sources during the late Pliocene (2.7 Ma). *Earth and Planetary Science Letters*, *317*, 8–19. https://doi.org/10.1016/j.epsl.2011.11.026

Nagashima, K., Tada, R., Tani, A., Sun, Y., Isozaki, Y., Toyoda, S., & Hasegawa, H. (2011). Millennial-scale oscillations of the westerly jet path during the last glacial period. *Journal of Asian Earth Sciences*, *40*(6), 1214–1220. https://doi.org/10.1016/j.jseaes.2010.08.010

Nie, J., Stevens, T., Rittner, M., Stockli, D., Garzanti, E., Limonta, M., et al. (2015). Loess plateau storage of northeastern Tibetan plateau-derived Yellow River sediment. *Nature Communications*, *6*(1), 1–10. https://doi.org/10.1038/ncomms9511

Nie, J., Stevens, T., Song, Y., King, J. W., Zhang, R., Ji, S., et al. (2014). Pacific freshening drives Pliocene cooling and Asian monsoon intensification. *Scientific Reports*, *4*(1), 5474. https://doi.org/10.1038/srep05474

Nier, A., & Schlutter, D. (1992). Extraction of helium from individual interplanetary dust particles by step-heating. *Meteoritics*, *27*(2), 166–173. https://doi.org/10.1111/j.1945-5100.1992.tb00744.x

Olivarez, A. M., Owen, R. M., & Rea, D. K. (1991). Geochemistry of eolian dust in Pacific pelagic sediments: Implications for paleoclimatic interpretations. *Geochimica et Cosmochimica Acta*, *55*(8), 2147–2158. https://doi.org/10.1016/0016-7037(91)90093-k

Ozima, M., & Podosek, F. A. (1983). *Noble gas geochemistry*. Cambridge University Press.

Patterson, D. B., & Farley, K. (1998). Extraterrestrial ^{3}He in seafloor sediments: Evidence for correlated 100 Kyr periodicity in the accretion rate of interplanetary dust, orbital parameters, and Quaternary climate. *Geochimica et Cosmochimica Acta*, *62*(23–24), 3669–3682. https://doi.org/10.1016/s0016-7037(98)00263-4

Patterson, D. B., Farley, K., & Norman, M. (1999). ^{4}He as a tracer of continental dust: A 1.9 million year record of aeolian flux to the west equatorial Pacific Ocean. *Geochimica et Cosmochimica Acta*, *63*(5), 615–625. https://doi.org/10.1016/s0016-7037(99)00077-0

Pullen, A., Kapp, P., & Chen, N. (2018). Development of stratigraphically controlled, eolian-modified unconsolidated gravel surfaces and yardang fields in the wind-eroded Hami Basin, northwestern China. *GSA Bulletin*, *130*(3–4), 630–648. https://doi.org/10.1130/b31734.1

Pullen, A., Kapp, P., McCallister, A. T., Chang, H., Gehrels, G. E., Garzione, C. N., et al. (2011). Qaidam Basin and northern Tibetan Plateau as dust sources for the Chinese Loess Plateau and paleoclimatic implications. *Geology*, *39*(11), 1031–1034. https://doi.org/10.1130/g32296.1

Qiang, M., Stevens, T., Li, G., Hu, L., Wang, X., Lang, W., & Chen, J. (2021). Late Quaternary dust, loess and desert dynamics in upwind areas of the Chinese Loess Plateau. *Frontiers in Earth Science*, *9*, 661874. https://doi.org/10.3389/feart.2021.661874

Rea, D. K., & Hovan, S. A. (1995). Grain size distribution and depositional processes of the mineral component of abyssal sediments: Lessons from the North Pacific. *Paleoceanography*, *10*(2), 251–258. https://doi.org/10.1029/94pa03355

Rea, D. K., & Leinen, M. (1988). Asian aridity and the zonal westerlies: Late Pleistocene and Holocene record of eolian deposition in the northwest Pacific Ocean. *Palaeogeography, Palaeoclimatology, Palaeoecology*, *66*(1–2), 1–8. https://doi.org/10.1016/0031-0182(88)90076-4

Rea, D. K., Snoeckx, H., & Joseph, L. H. (1998). Late Cenozoic eolian deposition in the North Pacific: Asian drying, Tibetan uplift, and cooling of the Northern Hemisphere. *Paleoceanography*, *13*(3), 215–224. https://doi.org/10.1029/98pa00123

Roe, G. (2009). On the interpretation of Chinese loess as a paleoclimate indicator. *Quaternary Research*, *71*(2), 150–161. https://doi.org/10.1016/j.yqres.2008.09.004

Sakuyama, M., & Nesbitt, R. (1986). Geochemistry of the Quaternary volcanic rocks of the northeast Japan arc. *Journal of Volcanology and Geothermal Research*, *29*(1–4), 413–450. https://doi.org/10.1016/0377-0273(86)90053-3

Serno, S., Winckler, G., Anderson, R. F., Hayes, C. T., McGee, D., Machalett, B., et al. (2014). Eolian dust input to the subarctic North Pacific. *Earth and Planetary Science Letters*, *387*, 252–263. https://doi.org/10.1016/j.epsl.2013.11.008

Serno, S., Winckler, G., Anderson, R. F., Jaccard, S. L., Kienast, S. S., & Haug, G. H. (2017). Change in dust seasonality as the primary driver for orbital-scale dust storm variability in East Asia. *Geophysical Research Letters*, *44*(8), 3796–3805. https://doi.org/10.1002/2016gl072345

Shao, Y., & Dong, C. (2006). A review on East Asian dust storm climate, modelling and monitoring. *Global and Planetary Change*, *52*(1–4), 1–22. https://doi.org/10.1016/j.gloplacha.2006.02.011

Shen, X., Wan, S., France-Lanord, C., Clift, P. D., Tada, R., Révillon, S., et al. (2017). History of Asian eolian input to the Sea of Japan since 15 Ma: Links to Tibetan uplift or global cooling? *Earth and Planetary Science Letters*, *474*, 296–308. https://doi.org/10.1016/j.epsl.2017.06.053

Song, Y., Li, Y., Cheng, L., Zong, X., Kang, S., Ghafarpour, A., et al. (2021). Spatio-temporal distribution of Quaternary loess across Central Asia. *Palaeogeography, Palaeoclimatology, Palaeoecology*, *567*, 110279. https://doi.org/10.1016/j.palaeo.2021.110279

Stevens, T., Buylaert, J.-P., Thiel, C., Újvári, G., Yi, S., Murray, A., et al. (2018). Ice-volume-forced erosion of the Chinese Loess Plateau global Quaternary stratotype site. *Nature Communications*, *9*(1), 1–12. https://doi.org/10.1038/s41467-018-03329-2

Sun, D., Su, R., Bloemendal, J., & Lu, H. (2008). Grain-size and accumulation rate records from Late Cenozoic aeolian sequences in northern China: Implications for variations in the East Asian winter monsoon and westerly atmospheric circulation. *Palaeogeography, Palaeoclimatology, Palaeoecology*, *264*(1–2), 39–53. https://doi.org/10.1016/j.palaeo.2008.03.011

Sun, Y., & An, Z. (2005). Late Pliocene-Pleistocene changes in mass accumulation rates of eolian deposits on the central Chinese Loess Plateau. *Journal of Geophysical Research*, *110*(D23), D23101. https://doi.org/10.1029/2005jd006064

Sun, Y., An, Z., Clemens, S. C., Bloemendal, J., & Vandenberghe, J. (2010). Seven million years of wind and precipitation variability on the Chinese Loess Plateau. *Earth and Planetary Science Letters*, *297*(3–4), 525–535. https://doi.org/10.1016/j.epsl.2010.07.004

Tagliabue, A., Bowie, A. R., Boyd, P. W., Buck, K. N., Johnson, K. S., & Saito, M. A. (2017). The integral role of iron in ocean biogeochemistry. *Nature*, *543*(7643), 51–59. https://doi.org/10.1038/nature21058

Takahashi, T., Hirahara, Y., Miyazaki, T., Senda, R., Chang, Q., Kimura, J.-I., & Tatsumi, Y. (2012). Primary magmas at the volcanic front of the NE Japan arc: Coeval eruption of crustal low-K tholeiitic and mantle-derived medium-K calc-alkaline basalts at Azuma volcano. *Journal of Petrology*, *54*(1), 103–148. https://doi.org/10.1093/petrology/egs065

Tanaka, T. Y., & Chiba, M. (2006). A numerical study of the contributions of dust source regions to the global dust budget. *Global and Planetary Change*, *52*(1–4), 88–104. https://doi.org/10.1016/j.gloplacha.2006.02.002

Tang, Y., Wan, S., Clift, P. D., Zhao, D., Xu, Z., Zhang, J., et al. (2022). Northward shift of the Northern Hemisphere westerlies in the early to late Miocene and its links to Tibetan uplift. *Geophysical Research Letters*, *49*(18), e2022GL099311. https://doi.org/10.1029/2022gl099311

Trusenkova, O., & Ishida, H. (2005). Seasonal variation of surface and deep currents in the Japan Sea. *Doboku Gakkai Ronbunshu*, *2005*(796), 796_93–796_111. https://doi.org/10.2208/jscej.2005.796_93

Uno, I., Eguchi, K., Yumimoto, K., Takemura, T., Shimizu, A., Uematsu, M., et al. (2009). Asian dust transported one full circuit around the globe. *Nature Geoscience*, *2*(8), 557–560. https://doi.org/10.1038/ngeo583

Venti, N. L., & Billups, K. (2012). Stable-isotope stratigraphy of the Pliocene–Pleistocene climate transition in the northwestern subtropical Pacific. *Palaeogeography, Palaeoclimatology, Palaeoecology*, *326*, 54–65. https://doi.org/10.1016/j.palaeo.2012.02.001

Wang, F., Sun, D., Chen, F., Bloemendal, J., Guo, F., Li, Z., et al. (2015). Formation and evolution of the Badain Jaran Desert, North China, as revealed by a drill core from the desert centre and by geological survey. *Palaeogeography, Palaeoclimatology, Palaeoecology*, *426*, 139–158. https://doi.org/10.1016/j.palaeo.2015.03.011

Wang, N., Jiang, D., & Lang, X. (2018). Northern westerlies during the Last Glacial Maximum: Results from CMIP5 simulations. *Journal of Climate*, *31*(3), 1135–1153. https://doi.org/10.1175/jcli-d-17-0314.1

Westerhold, T., Marwan, N., Drury, A. J., Liebrand, D., Agnini, C., Anagnostou, E., et al. (2020). An astronomically dated record of Earth's climate and its predictability over the last 66 million years. *Science*, *369*(6509), 1383–1387. https://doi.org/10.1126/science.aba6853

Winckler, G., Anderson, R. F., & Schlosser, P. (2005). Equatorial Pacific productivity and dust flux during the mid-Pleistocene climate transition. *Paleoceanography*, *20*(4), PA4025. https://doi.org/10.1029/2005pa001177

Woodard, S. C., Rosenthal, Y., Miller, K. G., Wright, J. D., Chiu, B. K., & Lawrence, K. T. (2014). Antarctic role in Northern Hemisphere glaciation. *Science*, *346*(6211), 847–851. https://doi.org/10.1126/science.1255586

Wu, F., Fang, X., Ma, Y., Herrmann, M., Mosbrugger, V., An, Z., & Miao, Y. (2007). Plio–Quaternary stepwise drying of Asia: Evidence from a 3-Ma pollen record from the Chinese Loess Plateau. *Earth and Planetary Science Letters*, *257*(1–2), 160–169. https://doi.org/10.1016/j.epsl.2007.02.029

Xu, Z., Li, T., Clift, P. D., Lim, D., Wan, S., Chen, H., et al. (2015). Quantitative estimates of Asian dust input to the western Philippine Sea in the mid-late Quaternary and its potential significance for paleoenvironment. *Geochemistry, Geophysics, Geosystems*, *16*(9), 3182–3196. https://doi.org/10.1002/2015gc005929

Xu, Z., Stevens, T., Yi, S., Mason, J. A., & Lu, H. (2018). Seesaw pattern in dust accumulation on the Chinese Loess Plateau forced by late glacial shifts in the East Asian monsoon. *Geology*, *46*(10), 871–874. https://doi.org/10.1130/g45105.1

Zeng, L., Lu, H., Yi, S., Li, Y., Lv, A., Zhang, W., et al. (2016). New magnetostratigraphic and pedostratigraphic investigations of loess deposits in north-east China and their implications for regional environmental change during the Mid-Pleistocene climatic transition. *Journal of Quaternary Science*, *31*(1), 20–32. https://doi.org/10.1002/jqs.2829

Zhang, B., Tsunekawa, A., & Tsubo, M. (2008). Contributions of sandy lands and stony deserts to long-distance dust emission in China and Mongolia during 2000–2006. *Global and Planetary Change*, *60*(3–4), 487–504. https://doi.org/10.1016/j.gloplacha.2007.06.001

Zhang, D., Wang, G., Abell, J. T., Pullen, A., Winckler, G., Schaefer, J. M., & Shen, T. (2022). Quantifying late Pleistocene to Holocene erosion rates in the Hami Basin, China: Insights into Pleistocene dust dynamics of an East Asian stony desert. *Geophysical Research Letters*, *49*(8), e2021GL097495. https://doi.org/10.1029/2021gl097495

Zhang, D., Wang, G., Pullen, A., Abell, J. T., Ji, J., & Shen, T. (2020). Landscape evolution and development of eolian-modified unconsolidated gravel surfaces and yardangs in the Hami Basin, China. *Geomorphology*, *368*, 107355. https://doi.org/10.1016/j.geomorph.2020.107355

Zhang, J., Hao, Q., & Li, S. H. (2022). An absolutely dated record of climate change over the last three glacial–interglacial cycles from Chinese loess deposits. *Geology*, *50*(10), 1116–1120.

Zhang, H., Nie, J., Liu, X., Pullen, A., Li, G., Peng, W., & Zhang, H. (2021). Spatially variable provenance of the Chinese Loess Plateau. *Geology*, *49*(10), 1155–1159. https://doi.org/10.1130/g48867.1

Zhang, Q., Liu, Q., Roberts, A. P., Larrasoaña, J. C., Shi, X., & Jin, C. (2020a). Mechanism for enhanced eolian dust flux recorded in North Pacific Ocean sediments since 4.0 Ma: Aridity or humidity at dust source areas in the Asian interior? *Geology*, *48*(1), 77–81. https://doi.org/10.1130/g46862.1

Zhang, Q., Liu, Q., & Sun, Y. (2020b). Review of recent developments in aeolian dust signals of sediments from the North Pacific Ocean based on magnetic minerals. *Geological Magazine*, *157*(5), 790–805. https://doi.org/10.1017/s0016756819000712

Zhang, W., Chen, J., Ji, J., & Li, G. (2016). Evolving flux of Asian dust in the North Pacific Ocean since the late Oligocene. *Aeolian Research*, *23*, 11–20. https://doi.org/10.1016/j.aeolia.2016.09.004

Zhang, W., Li, G., & Chen, J. (2020). The application of Neodymium isotope as a chronostratigraphic tool in North Pacific sediments. *Geological Magazine*, *157*(5), 768–776. https://doi.org/10.1017/s001675681900089x

Zhang, X.-Y., Gong, S., Zhao, T., Arimoto, R., Wang, Y., & Zhou, Z. (2003). Sources of Asian dust and role of climate change versus desertification in Asian dust emission. *Geophysical Research Letters*, *30*(24), 2272. https://doi.org/10.1029/2003gl018206

Zhang, Y. G., Ji, J., Balsam, W., Liu, L., & Chen, J. (2009). Mid-Pliocene Asian monsoon intensification and the onset of Northern Hemisphere glaciation. *Geology*, *37*(7), 599–602. https://doi.org/10.1130/g25670a.1

Zhao, H., Sun, Y., & Qiang, X. (2022). Mid-Pleistocene formation of modern-like desert landscape in North China. *Catena*, *216*, 106399. https://doi.org/10.1016/j.catena.2022.106399

References From the Supporting Information

Bailey, J. C. (1993). Geochemical history of sediments in the northwestern Pacific Ocean. *Geochemical Journal*, *27*(2), 71–90. https://doi.org/10.2343/geochemj.27.71

Farley, K. A. (2001). Extraterrestrial helium in seafloor sediments: Identification, characteristics, and accretion rate over geologic time. In *Accretion of extraterrestrial matter throughout Earth's history* (pp. 179–204). Springer.

Mamyrin, B. A., & Tolstikhin, I. N. (1984). *Helium isotopes in nature*. Elsevier.

Weber, E. T., Owen, R. M., Dickens, G. R., Halliday, A. N., Jones, C. E., & Rea, D. K. (1996). Quantitative resolution of eolian continental crustal material and volcanic detritus in North Pacific surface sediment. *Paleoceanography*, *11*(1), 115–127. https://doi.org/10.1029/95pa02720